### Title

Fine spatial structure of genetically distinct picocyanobacterial populations across environmental gradients in the Costa Rica Dome




### Journal

Limnology and Oceanography, 59(3)

### ISSN

0024-3590



### Authors

Gutiérrez-Rodríguez, Andrés
Slack, Gillian
Daniels, Emy F
et al.



### Publication Date

2014-05-01

### DOI

10.4319/lo.2014.59.3.0705

Peer reviewed

*Limnol. Oceanogr.*, 59(3), 2014, 705–723

doi:10.4319/lo.2014.59.3.0705

# Fine spatial structure of genetically distinct picocyanobacterial populations across environmental gradients in the Costa Rica Dome

Andrés Gutiérrez-Rodríguez ,[1,a,*] Gillian Slack,[1] Emy F. Daniels,[1] Karen E. Selph,[2] Brian Palenik,[1] and Michael R. Landry [1]

[1] Scripps Institution of Oceanography, University of California at San Diego, La Jolla, California
[2] Department of Oceanography, University of Hawaii at Manoa, Honolulu, Hawaii

*Abstract*

We investigated the spatial variability of picocyanobacterial community structure across the Costa Rica Dome (CRD), an offshore upwelling system characterized by high seasonal abundance of *Synechococcus* spp. We constructed clone libraries of the *rpoC1* gene to survey picocyanobacterial diversity and developed specific real-time quantitative polymerase chain reaction assays to assess the distribution of genetically distinct *Synechococcus* (SYN) and *Prochlorococcus* (PRO) populations across vertical and horizontal physicochemical gradients. Flow cytometry data showed that cell abundances for both SYN and PRO were highest near the dome center. Phylogenetic analysis of *rpoC1* sequences revealed a remarkably high and distinctive picocyanobacterial diversity (FLU1-3, CRD1, Clade II, XV, XVI) that included "novel" SYN and PRO genotypes. Furthermore, genetically different populations exhibited vertical and horizontal spatial partitioning. Abundances of distinct SYN genotypes peaked at subsequent depth horizons, leading to a fine vertical structure with at least three populations stacked within the upper 30–40 m at the dome. Clade II and FLU1A peaked in surface waters, while maximum concentrations of CRD1, FLU1B, and Clade XVI occurred in the upper and lower thermocline, respectively. Horizontally, Clade II abundance in surface waters remained high across the entire region, while SYN genotypes CRD1 and FLU1A increased with shoaling of the thermo- and nutricline toward the center of the dome to become the dominant genotypes of the SYN assemblage in the dome. Below the mixed layer, Clade XVI and PRO genotype FLU2, virtually absent outside the dome, became abundant components of the picocyanobacterial assemblage. Despite their phylogenetic relatedness, FLU1A and FLU1B subclades followed different distributional patterns, suggesting ecological significance of the microdiversity within the clade. The unprecedented fine vertical structure demonstrated for SYN genotypes is driven by sharp physicochemical gradients (e.g., density, nutrient, oxygen, and trace metals) created by the dome and the presence of a shallow oxycline that enhances habitat diversification.

Marine picocyanobacteria of the genera *Synechococcus* (SYN) and *Prochlorococcus* (PRO) dominate photosynthetic biomass and productivity across vast regions of the oceans and constitute a major component of the global carbon cycle (Li 1994; Jardillier et al. 2010). Despite their phylogenetic proximity, SYN and PRO follow different spatial distributions, both horizontally and vertically, that reflect their distinct ecophysiological preferences (Ferris and Palenik 1998; Partensky et al. 1999; Scanlan and West 2002). PRO distribution, for instance, is constrained to warm oligotrophic, typically open-ocean waters between 45°N and 42°S. SYN is distributed more ubiquitously, including tropical and boreal seas as well as sub-Antarctic waters (Doolittle et al. 2008; Scanlan et al. 2009), and its abundance is usually highest near the coast, declining toward oligotrophic oceanic conditions (Waterbury et al. 1979; Olson et al. 1990; Scanlan et al. 2009). While both genera may coexist in the same water column, maximum SYN concentration is often confined to the upper euphotic zone, while PRO distribution extends much deeper (Partensky et al. 1999).

The ecological importance and versatility of PRO and SYN are likely rooted in their significant genetic diversity (Palenik 1994; Rocap et al. 2002; Scanlan et al. 2009). For PRO, genetically and physiologically distinct populations divide the full depth range of the euphotic zone according to their specific habitat preferences for light and nutrients (Moore and Chisholm 1999; Rocap et al. 2003). Similarly, environmental populations of SYN (Ferris and Palenik 1998; Mühling et al. 2006; Huang et al. 2011) and clonal isolates (Fuller et al. 2003; Mazard et al. 2012) display large genetic and physiological diversity that likely explains the capacity of the genus to thrive across contrasting oceanographic conditions. The ecological significance of this genetic diversity is inferred by the coherence of SYN genotypic composition with respect to environmental niches occupied in geographically distant ecosystems (Zwirglmaier et al. 2007, 2008). Molecular quantitative approaches have further revealed consistent spatial (Fuller et al. 2006; Paerl et al. 2011*a*; Tai et al. 2011) and temporal (Tai and Palenik 2009; Paerl et al. 2011*b*; Post et al. 2011) distributional patterns among genotypes that reflect their different habitat preferences. However, the ecophysiological properties that determine the ecological niches of specific genotypes and the environmental factors regulating their distributions and dynamics are not fully understood.

The Costa Rica Dome (CRD) is a 300–500 km open-ocean upwelling center in the eastern tropical Pacific, typically around 9°N, 90°W, where strong opposing east–west currents, seasonal winds, and the continental margin

* Corresponding author: agutierrez@sb-roscoff.fr

[a] Present addresses: Université Pierre et Marie and Centre National de la Recherche Scientifique, UMR7144 Station Biologique, Roscoff, France

boundary of Central America combine to cause the eastern shoaling of the North Equatorial Counter Current thermocline ridge (Wyrtki 1964; Fiedler and Talley 2006). The CRD evolves seasonally from coastal waters off Nicaragua and Costa Rica to reach a mature state in terms of offshore extension and minimum thermocline depth during summer (Fiedler 2002). Extraordinary densities of *Synechococcus* spp., often exceeding $10^6$ cells $mL^{-1}$ (Li et al. 1983; Saito et al. 2005), are a unique aspect of the CRD summertime state, in striking contrast with the general dominance of eukaryotic primary producers in upwelling systems. Specific factors underlying the competitive advantage of SYN in the region are not fully understood, but experimental evidence indicates that the trace-metal chemistry of the system plays a key role in structuring the photosynthetic community (Franck et al. 2003; Saito et al. 2005).

In addition to its direct fertilization effect, isopycnal doming in the CRD compresses vertical physicochemical gradients (e.g., temperature, salinity, oxygen, and trace metals) within the euphotic zone, which, in combination with the shallow oxygen minimum zone of the region, generates a marked vertical structure with high potential for niche diversification. The only previous study of SYN diversity in the region focused on the mixed layer, where two novel SYN lineages, CRD1 and CRD2, were found to dominate (Saito et al. 2005). Here we expand on this seminal study by assessing quantitative changes in picocyanobacterial diversity for a depth-resolved transect crossing the CRD and surrounding waters. The main objectives of this study are to explore picocyanobacterial diversity and the mechanisms governing niche partitioning among phylogenetically closely related SYN and PRO populations, taking advantage of the CRD's high cell abundances and sharp physicochemical gradients. The specific questions and issues that we address in this context are (1) Is the dominant seasonal bloom-forming population of SYN genetically distinct from background populations in oligotrophic waters? (2) How is the spatial structure of the picocyanobacterial community influenced by strong physicochemical gradients in the vertical and horizontal domains associated with the presence of the dome? (3) What is the potential ecological significance of the genetic diversity, as reflected in population-specific habitat associations?

## Methods

*Study area and sample collection*—We sampled the CRD upwelling region (Fig. 1) on R/V *Melville* cruise MV1008 (22 June–25 July 2010) as part of the CRD flux and zinc experiments (FLUZiE) project, which had the broad goals of characterizing plankton community structure, biogeochemical fluxes, and mechanisms of phytoplankton control in this ecosystem. For this specific study, we sampled stations along a ~ 500 km transect that crossed the CRD and among a grid of stations around the core of the dome (Fig. 1). Hydrographic data (temperature, salinity, fluorescence, and dissolved oxygen) and discrete water samples were acquired with a conductivity–temperature–depth rosette system with 24 of the 10 liter Niskin bottles with

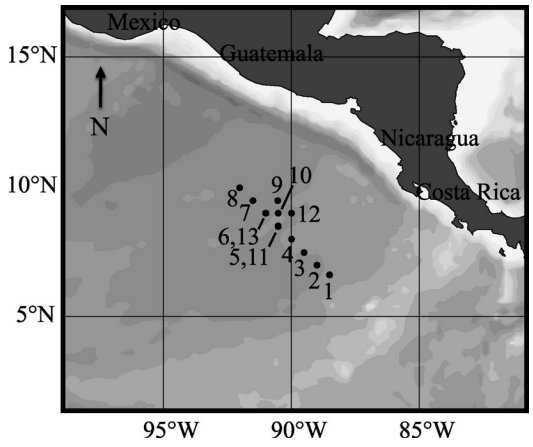


Fig. 1. Map of the Costa Rica Dome (CRD) sampling area showing station numbers and locations.

Teflon-coated springs. Seawater samples were collected from eight depths in the upper 80–120 m at each station, extending from the surface to the depth of penetration of ~ 0.1% surface irradiance ($I_0$). Each depth was sampled for nutrient, chlorophyll *a* (Chl *a*), flow cytometry (FCM), and deoxyribonucleic acid (DNA) analyses.

Nutrient samples were filtered directly from the Niskin bottle through an acid-washed rinsed 0.1 $\mu$m Suporcap filter capsule to 50 mL Falcon tubes. The tubes were rinsed twice, filled, immediately frozen (−20°C), and later analyzed for major nutrient concentrations ($NO_3^- + NO_2^-$, $NO_2^-$, $PO_4^{3-}$, $NH_4^+$, and $SiOH_3$) by flow injection by the Analytical Laboratory at the Marine Science Institute, University of California, Santa Barbara. Samples (250 mL) for Chl *a* were immediately filtered onto 25 mm glass fiber filters (Whatman GF/F), and the pigment was extracted with 90% acetone in a dark refrigerator for 24 h. Extracted samples were shaken, centrifuged, and quantified on a calibrated Turner Designs model 10 fluorometer (Landry et al. 2009).

For FCM analysis, 2 mL seawater samples were preserved with 0.5% paraformaldehyde (vol : vol, final concentration; Sigma Aldrich), flash-frozen in liquid nitrogen, and transferred to a −80°C freezer until analysis. For DNA analysis, we filtered 1–2 liters of seawater through 0.2 $\mu$m Supor filter discs of 47 mm diameter (Pall Life Sciences). The filters were folded and kept in 1.8 mL cryovials, flash-frozen, and stored at −80°C until analysis.

*Flow-cytometric analysis*—Cell abundances of SYN and PRO were measured using a Beckman–Coulter EPICS flow cytometer following the procedure described in Selph et al. (2011). Briefly, thawed samples were stained with Hoechst 33342 (1 $\mu$g $mL^{-1}$, vol : vol, final concentration) at room temperature in the dark for 1 h, and 100 $\mu$L aliquots were injected into the flow cytometer using a coupled Harvard Apparatus syringe pump for volumetric sample delivery. SYN and PRO populations were distinguished based on their chlorophyll *a* (red fluorescence, 680 nm), phycoerythrin (orange fluorescence, 575 nm), DNA (blue fluorescence, 450 nm), forward and 90° side-scatter signatures. Calibration beads (0.5 and 1.0 $\mu$m yellow-green beads and 0.5 $\mu$m ultraviolet beads) were used as fluorescence

Table 1. Real-time qPCR assay conditions for genetically distinct major populations of SYN and PRO found in the CRD.

| Name (SYN or PRO affiliation) | Primers | 5′- to 3′ (forward, reverse) | Annealing T (°C) | Amplicon size (bp) | Amplification efficiency | Standard curve ($R^2$) |
|---|---|---|---|---|---|---|
| CRD1 | rpoc599F | CCA CTC GTC CTC AGT AAG CAA | 68.5 | 220 | 0.88 | $Ct = 33.13 - 3.64 \times \log conc$ |
| (SYN) | rpoc730R | TGA AAG CCG GGT GCG CAG G | 68.5 | | | (0.999) |
| FLU1A | rpoc370F | GTC TTC CCG AAG CTG CTG G | 68.5 | 115 | 0.69 | $Ct = 40.07 - 4.39 \times \log conc$ |
| (SYN) | rpoc484R | CGC CGA GGA TTC AGA GAT T | 68.5 | | | (0.998) |
| FLU1B | rpoc466F | GAT CTC GGA ATC TTC CGC G | 68.5 | 100 | 0.82 | $Ct = 35.62 - 3.83 \times \log conc$ |
| (SYN) | rpoc565R | GGA TCC CGG CGA CCA CAA A | 68.5 | | | (0.999) |
| Clade XVI | rpoc601F | GAC ATC ACG CAG TGG CAT GTC | 62 | 94 | 0.98 | $Ct = 38.65 - 3.37 \times \log conc$ |
| (SYN) | rpoc694R | TAT CAA GCT GGC AGC TCC CGT | 62 | | | (0.998) |
| FLU2 | rpoc541F | AAG GTC TTG ATG ATC ACC TGT | 62 | 110 | 0.98 | $Ct = 30.40 - 3.350 \times \log conc$ |
| (PRO) | rpoc650R | GAA TCC CTA GCT ATG TGG CA | 62 | | | (0.998) |
| Clade II | rpoc378F | CTA CGT GCG CAT CCT GCT | 68.5 | 170 | 0.81 | $Ct = 35.76 - 3.87 \times \log conc$ |
| (SYN) | rpoc547R | TCG GAR TCT TCG GCG TAG ATC | 68.5 | | | (0.986) |
| FLU3 | rpoc529F | CTG CTT ATA TTT AAG ATC CTT A | 54 | 117 | 0.79 | $Ct = 38.65 - 3.37 \times \log conc$ |
| (PRO) | rpoc645R | CCT AGY TAY GTA CGW ATT TTV | 54 | | | (0.998) |

standards and raw data were processed using the software Flowjo (TreeStar, www.flowjo.com). Contour plots of FCM and hydrographic data were generated using a "VG gridding" algorithm in Ocean Data View (Schlitzer 2006).

*DNA extraction,* rpoC1 *amplification, cloning, and phylogenetic analysis*—DNA was extracted from organisms collected on the 0.2 $\mu$m Supor filter discs following the phenol-chloroform method described by Tai and Palenik (2009) with slight modifications, detailed below, due to the larger diameter of the filter used. The 47 mm filters were cut in half and chopped finely into $\sim 1 \times 5$ mm strips with a razor blade wiped in ethanol. For each half of the filter, proteins were removed through two extractions adding equal volumes of 25 : 24 : 1 phenol : chloroform : isoamyl alcohol, followed by a third one with 24 : 1 chloroform : isoamyl alcohol. The aqueous phases from the two halves of each filter were combined after the last extraction, and the DNA contained was purified using a silica gel column (Dneasy blood and tissue kit; Qiagen) doubling the amount of buffer AL and ethanol recommended by the manufacturer, and eluted into 400 $\mu$L of the manufacturer's buffer. Extracted DNA was quantified using PicoGreen fluorescent dye (Quant-iT, Qiagen) following the manufacturer's protocol.

Following a slightly modified protocol of that described by Tai and Palenik (2009), we constructed clone libraries of the *rpoC1* gene for samples collected from surface mixed layer and deeper waters from Sta. 2 (15 and 45 m) and Sta. 11 (2 and 30 m). Like Tai and Palenik (2009), we used the cyanobacterial-specific *rpoC1* primers, SAN-157F and SAC1039R, to amplify an 841 basepair (bp) fragment of the *rpoC1* gene. However, for polymerase chain reactions (PCR) and cycling, we used GoTaq® Green Mastermix (Promega) and 1 $\mu$mol $L^{-1}$ final concentration of forward and reverse primers. The PCR products were purified using the QIAquick® gel extraction kit (Qiagen) and cloned with the TOPO TA cloning kit pCR®2.1 (Invitrogen) following the manufacturer's protocol. Plasmid DNA was isolated ($\sim$ 25 clones for each library) using the QIAprep Spin Miniprep Kit (Qiagen) following the Invitrogen protocol, and the *rpoC1* inserted fragment was sequenced from both ends using the T3 and T7 sequencing primers provided by Invitrogen.

The *rpoC1* sequences were trimmed from the plasmid and aligned to publicly available *rpoC1* sequences from cultured isolates and environmental sequences of SYN and PRO using the CLC Genomics Workbench (CLC Bio). Phylogenetic relationships were explored using Molecular Evolutionary Genetic Analysis software (MEGA5; Tamura et al. 2011), and sequences were realigned using Multiple Sequence Comparison by Log-Expectation (MUSCLE) algorithms (Edgar 2004). A maximum likelihood consensus tree was built from distances calculated using the Tamura–Nei model (Tamura and Nei 1993) following the 50% majority rule after 1000 bootstrap replicates.

*Real-time quantitative PCR*—We designed specific pairs of primers targeting six genetically distinct groups of picocyanobacteria determined by the phylogenetic analysis of the clone libraries (4 SYN and 2 PRO; Table 1) and SYN Clade II primers published in Tai and Palenik (2009). Primers were manually designed to maximize the coverage of targeted groups (i.e., minimizing the number of mismatches at the 3′ end) while minimizing the amplification from nontargeted groups (i.e., maximizing number of mismatches with sequences from nontargeted groups). Specificities of the primers were experimentally optimized by testing their ability to amplify target and nontarget plasmid DNA under a range of annealing temperatures. The presence of a single band corresponding to the PCR product of the target plasmid DNA at the end of a 40-cycle end-point PCR indicated the specificity of the primers. To further ensure specificities, we performed analogous cross-reactivity tests for each of the specific assays. We optimized the quantitative polymerase chain reaction (qPCR) conditions so the amplification signal yielded by reactions containing nonspecific DNA standards was lower than 0.1% of the signal obtained in reactions initiated with the same concentration of standard DNA targeted by the primer set (*see* below).

Reactions for qPCR (25 $\mu$L) were prepared by combining 12.5 $\mu$L of GoTaq® qPCR Mastermix (Promega), 2.5 $\mu$L

of forward and reverse primers stock (100 $\mu$mol $L^{-1}$), 2.5 $\mu$L template DNA, and nuclease free water to a final 25 $\mu$L volume. Potential PCR inhibition was tested by serial dilution of the DNA templates, but it was not observed for the range of DNA concentrations in our field samples. Real-time SYBR green fluorescence data were acquired using a Rotor-Gene Q machine (Qiagen) during the thermocycling protocol that included 10 min at 95°C followed by 40 cycles at 95°C for 30 s, the corresponding clade-specific annealing temperature for 30 s, followed by 30 s at 72°C, to finish with 95°C for 1 min. To assess the melting temperature of the amplified product, we programmed a ramp down to 55°C followed by a ramp up to 95°C at a 1°C $min^{-1}$ rate.

Standards were prepared using plasmid circular DNA with specific *rpoC1* inserts representative of each of the targeted picocyanobacterial groups determined from the clone libraries. To take into account the influence of the DNA conformation for qPCR performance (Hou et al. 2010), we prepared linear standards by incubating the circular plasmid DNA (10 $\mu$L) with Nco1 restriction nuclease (New England BioLabs) for 6 h at 37°C followed by 30 min at 65°C to inactivate the enzyme. Digested plasmid DNA was purified (QIAquick, PCR Purification Kit, Qiagen), and linearization of the circular plasmid was verified by running a subsample of the digested and original circular plasmid on an agarose gel. Although the mechanism was unclear, running the linear DNA through agarose gel biased the subsequent qPCR reactions, leading to consistent overestimation of the estimated number of *rpoC1* copies for all specific groups. Accordingly, we only used linearized DNA that did not undergo agarose gel purification as standard in the qPCR assays. DNA concentration was quantified using PicoGreen fluorescent dye as described above, and serial dilutions of the standards ($\times$10 fold) with concentrations (*rpoC1* copies per reaction) spanning at least 6 orders of magnitude were run for each specific qPCR assay (Table 1). The baseline and threshold cycle (Ct) were estimated automatically with the Rotor-Gene Q Series software (version 1.7) provided by the manufacturer. The coefficient of determination of the standard curve was above 0.99 for all specific assays (Table 1). This linearity was used to assess the concentration of *rpoC1* copies from measured Ct in unknown environmental samples.

*Correlation and multidimensional scaling analysis*—To better understand how physicochemical gradients associated with the dome influence spatial structure of the picocyanobacterial community, we analyzed the relationships between qPCR determined abundance of specific SYN and PRO subpopulations and environmental factors using pairwise correlation analysis and multidimensional scale-ordination techniques. All data were log $(x + 1)$ transformed before the analyses and plots. Nonmetric multidimensional scaling analysis (nMDS) seeks an ordination plot in which the distance between all pairs of samples are maximized while maintaining the same rank order with their dissimilarities in species composition. A matrix of Bray–Curtis dissimilarities was calculated and subjected to nMDS in 2–3 dimensions configuration. The correlations between the two dimensional configuration (scores) and environmental variables were calculated and represented in the nMDS plot as arrows of length and direction proportional to the strength and sign of the correlation, respectively. JMP version 9 (SAS Institute) and Paleontological Statistics (PAST; Hammer et al. 2001) software packages were used for pairwise correlation and nMDS analysis, respectively.

*Nucleotide sequence accession numbers*—The sequences reported in this study have been deposited in the GenBank database under the following accession numbers: KF113588–KF113680.

## Results

*Oceanographic conditions*—CRD upwelling is shown by the shoaling of the thermocline and the halocline in Fig. 2. This doming considerably reduces the mixed-layer depth compared with the oligotrophic waters surrounding the dome and compresses the isoclines, creating sharp vertical physicochemical gradients within the euphotic zone (Fig. 2). For instance, temperature declined dramatically ($\sim$ 10°C) with depth within the first 30 m for stations at the core of the dome but not for stations outside (Fig. 2). Nonetheless, surface temperature was observed to be relatively constant ($\sim$ 27.5°C) along the transect in and out of the dome.

Salinity follows a similar pattern as temperature, with the doming of the isohalines bringing saltier waters into shallower depths ($\sim$ 20–40 m) but without clearly reaching the surface mixed layer. The surface salinity gradient observed was in fact dominated by the presence of a saltier water mass northwestward of the transect (Fig. 2), in agreement with climatological data of the region (Fiedler and Talley 2006). Upwelling conditions are also reflected in the shallower nitracline observed in the dome ($\sim$ 20 m) compared with its deeper position outside ($\sim$ 40 m; Fig. 2). For instance, the depth of the nitracline ($\sim$ 15 $\mu$mol $L^{-1}$ $NO_3^-$ isoclines) was at $>$ 20% surface irradiance ($I_0$) near the dome center, but below the 2% isolume at Stas. 1–3 located outside of the dome, although light penetration was similar. The doming of the isoclines can therefore bring waters of distinct chemistry into the euphotic zone, generating new habitats for photosynthetic organisms unavailable in background oligotrophic waters (*see* Discussion). The distribution of $PO_4^{3-}$ followed that of $NO_3^-$ ($R^2 = 0.992$, $p < 0.0001$, $n = 102$). Chl *a* concentration showed a subsurface maxima that followed the thermocline along the transect (Fig. 2). Chl *a* was highest for the dome stations at $\sim$ 20 m depth (0.5 $\mu$g Chl *a* $L^{-1}$). Although the depth of this maximum deepened outside of the dome, its magnitude did not decline appreciably (0.4 $\mu$g Chl *a* $L^{-1}$ at 60 m; Fig. 2).

*Distributions of picocyanobacteria from FCM*—Abundances of SYN and PRO were both highest in the dome (90–91°W), but their spatial distributions were different (Fig. 2). Whereas surface concentrations of SYN increased

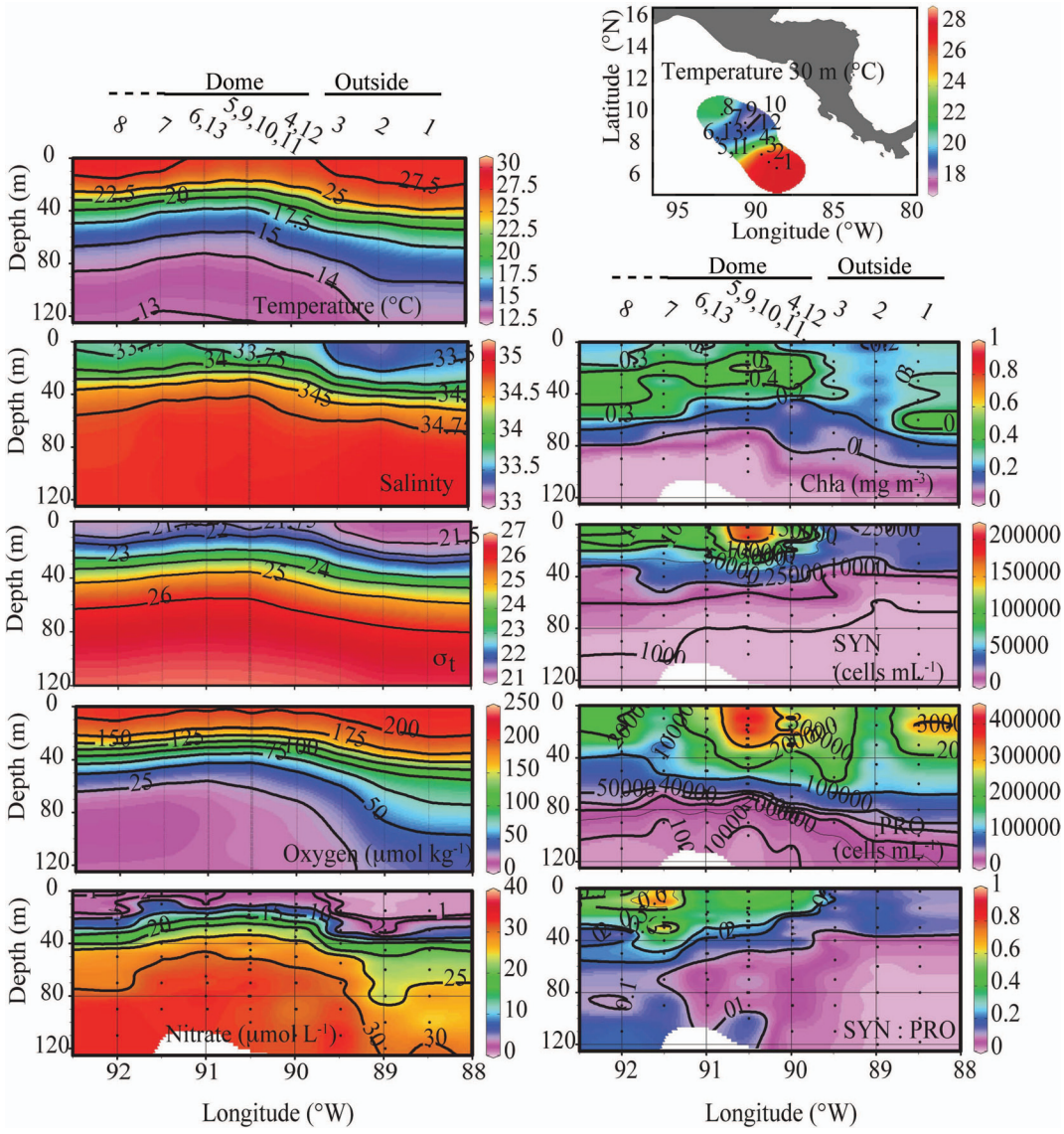


Fig. 2. Depth profiles of water temperature (°C), salinity, density ($\sigma_t$), oxygen ($\mu$mol kg$^{-1}$), nitrate ($\mu$mol L$^{-1}$), *Synechococcus* (SYN, cells mL$^{-1}$), and *Prochlorococcus* abundances (PRO, cells mL$^{-1}$), and SYN : PRO abundance ratio in CRD stations along the transect in the upper 120 m, and a map showing the station locations superposed on the 30 m depth isotherm. Station numbers indicate their positions on the transect.

more than fivefold from 25,000 cells mL$^{-1}$ at Stas. 1–3 to ~ 200,000 cells mL$^{-1}$ at Stas. 9–11, PRO increased only moderately (1.5 to 2-fold) to a ~ 500,000 cells mL$^{-1}$ maximum in the dome. Abundances of SYN and PRO both declined northwest of the transect, although this decrease was more marked for PRO, which reached minimum concentrations at Stas. 7–8 (~ 100,000 cells mL$^{-1}$; Fig. 2). As a consequence, the highest SYN : PRO abundance ratio did not coincide with maximum SYN abundance in the dome but was instead found northwestward of the dome (Fig. 2), in agreement with previous observations (Fig. 2B in Saito et al. 2005). As expected, SYN and PRO also differed in vertical distributions, with SYN concentrations highest in the surface mixed layer and dramatically reduced below, while PRO spanned deeper in the water column (Fig. 2).

Distinct populations of SYN could be distinguished in the dome based on their phycoerythrin fluorescence (PE) assessed by flow cytometry. The high PE population was present at the surface and at 30 m, then disappeared so that only the low PE population remained present in deeper waters below the thermocline (Fig. 3).

*Picocyanobacterial* rpoC1 *diversity*—A total of 93 cyanobacterial *rpoC1* gene sequences were isolated from the surface mixed layer and subsurface waters at Sta. 11 (2 and 30 m) and Sta. 2 (15 and 45 m), representing the upwelling conditions of the CRD and more typical oligotrophic tropical ocean conditions surrounding the dome, respectively (Fig. 2). Phylogenetic analyses revealed that SYN phylotypes dominated the surface libraries (40 out of 48 total surface clones) while PRO phylotypes were

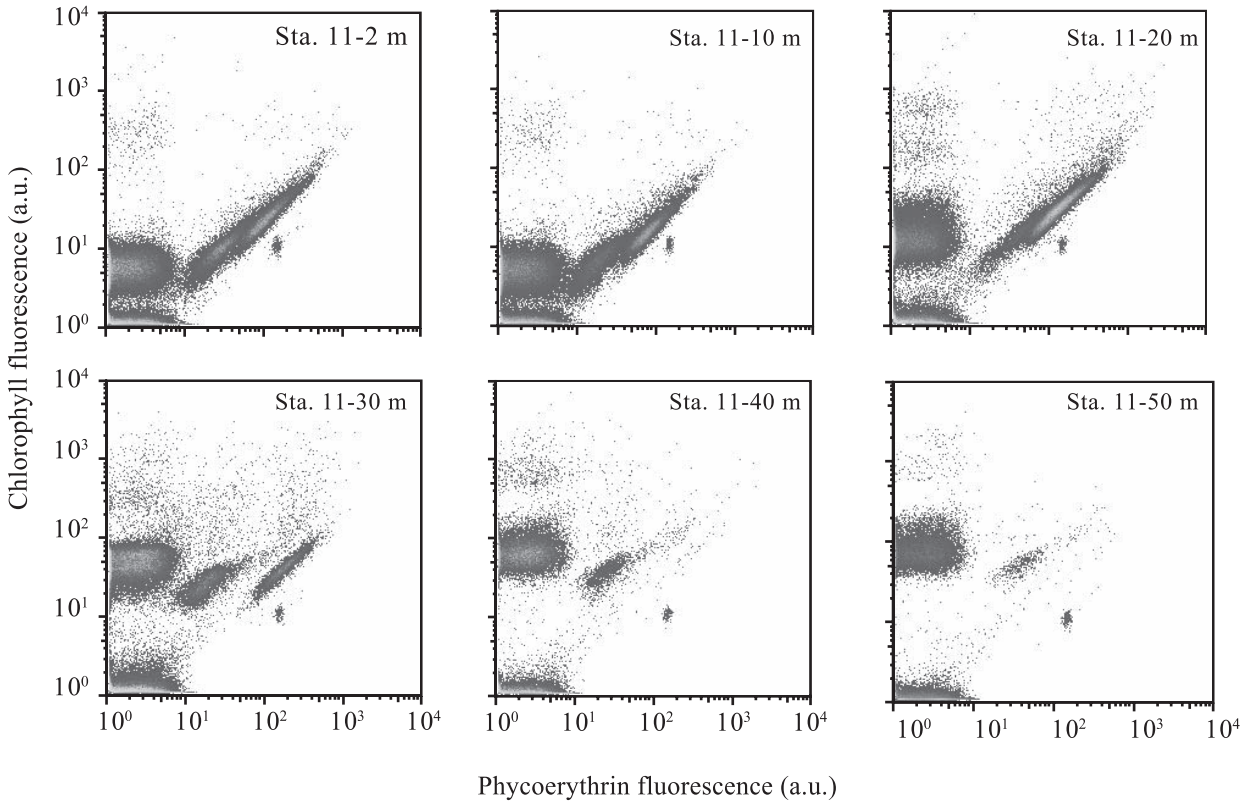


Fig. 3. Vertical structure of picophytoplankton populations defined by their chlorophyll vs. phycoerythin fluorescence (a.u.) in Sta. 11. at 2 m, 10 m, 20 m, 30 m, 40 m, and 50 m.

more abundant below the mixed layer (35 out of 45 total subsurface clones; Fig. 4). The majority of SYN clones were clustered in two major groups. One group contained sequences from both surface and subsurface waters that were closely related to MITS9220 and other isolates belonging to SYN CRD1 clade (Fig. 4). The other group, which we named FLU1, only contained sequences recovered from surface waters (57% of total SYN-like sequences collected from surface libraries) and formed a well-defined cluster without any known cultivated representative (Fig. 4). FLU1 could be separated further into FLU1A and FLU1B subclusters (Fig. 4). Despite the semiquantitative nature of clone libraries, the high percentage of sequences collected from the dome in FLU1A (59% of sequences within FLU1A subcluster) and from outside the dome in FLU1B (83% of sequences within FLU1B; Fig. 4), suggested a different distribution for each subgroup (*see* qPCR results). Both the presence of CRD1 and FLU1 groups, as well as FLU1A and 1B subgroups, were well supported by the bootstrap values (Fig. 4). The remaining SYN sequences collected from the dome clustered into two groups. One group contained only surface sequences that were most closely related to strain CC9605, belonging to SYN Clade II. The other group contained only sequences from subsurface waters that were most closely related to UW105 and UW140 belonging to SYN Clade XVI. Finally, Clade XV was represented in our library by a single sequence collected from subsurface waters within the dome (Fig. 4).

The few PRO-like sequences collected from surface waters clustered together regardless of their collection site and formed a subgroup closely related to eMIT9215, a high-light–adapted PRO clade. In contrast, PRO sequences recovered below the mixed layer formed two main groups, named FLU2 and FLU3, with different proportions of their sequences collected within and outside of the dome (Fig. 4). FLU2 comprised only sequences retrieved from the dome and were closely related ($>$ 98% *rpoC1* nucleotide similarity) yet remarkably distant from any known cultured representative or environmental isolate. FLU3 was most closely related to eNATL clade and contained mainly sequences collected from waters outside the dome ($>$ 80% of the FLU3 sequences). However, as observed for FLU1, FLU3 could be further divided into two subgroups differently enriched with sequences from the clone libraries sampled in and outside of the dome (Fig. 4).

*Specificity and coverage of qPCR assays*—We developed specific qPCR assays to assess the spatial distributions of major SYN and PRO subgroups determined by the clone libraries (Table 1). The majority of the clone sequences had perfect matches or single mismatches with the specific primers designed, and $\sim$ 80% of the sequences from the clone libraries were specifically amplified when tested in silico (Fig. 4). However, the proportion of environmental clones covered by the corresponding primer sets (i.e., $\leq$ 1 mismatch between sequence and reverse and forward primers together) differed among groups (Fig. 4). Overall,

the total SYN concentrations estimated from qPCR assays were in good agreement with those assessed with FCM (log SYN qPCR = 1.11 + 0.78 log SYN FCM, $R^2 = 0.77$, $p < 0.0001$) although the ratio of qPCR : FCM estimated SYN abundances ranged from 0.1 to 2.2. This discrepancy has been noted in previous studies, where the higher abundance of qPCR-based relative to FCM estimates was related to the presence of multiple genome copies (Tai and Palenik 2009; Ahlgren and Rocap 2012). The few samples exhibiting qPCR : FCM ratios < 1 came from subsurface waters, suggesting the inability of the general primers to cover the whole SYN diversity, leaving a fraction of the low-abundance SYN assemblage in deeper waters out of the reach of qPCR-based abundance estimates. Overall, the observed qPCR : FCM ratio variability is consistent with the range reported in previous studies and at levels significantly lower than the clade-specific abundance and spatial distributions.

Results from cross-reactivity tests performed between specific primer sets and plasmid DNA from targeted and nontargeted groups indicated the specificity of the qPCR assays (Fig. 5). The Ct of those reactions containing nontargeted DNA was equal to or higher than the Ct obtained for reactions containing targeted DNA at three orders of magnitude lower concentration (Web Appendix, www.aslo.org/lo/toc/vol_59/issue_3/0705a.html). In other words, contamination of the signal by cross-reaction with nontargeted DNA remained below 0.1% for the newly developed qPCR assays. In the case of Clade II specific primers, there was a higher degree of cross-reactivity with clones from nontargeted CRD1, FLU1A, and 1B groups that increased the contamination threshold to 1% (i.e., given the same starting concentration for each specific group, 1% of the signal obtained for Clade II would be due to these nontargeted genotypes), while in silico analysis suggested potential cross-reactivity with closely related Clade XV. To further test the specificity of Clade II assay on CRD samples, we built a clone library with the qPCR product of two surface samples amplified with this set of primers. We sequenced 10 clones, all of which clustered together with cultured and environmental sequences belonging to Clade II (data not shown), which confirmed the specificity of Clade II qPCR assay in our study. The presence of a single peak in the melting curve provided further support to the specificity of the assays. The variability among replicates was on average low for all specific qPCR reactions using both plasmid standards and field DNA samples, with Ct differing less than 0.2 units (mean Ct CVP < 3%) and supported the reproducibility of the assays.

*Horizontal and vertical distribution of picocyanobacterial lineages determined by qPCR*—The specific qPCR assays applied to four depth-resolved profiles revealed different distributional patterns of SYN and PRO lineages in the CRD upwelling and surrounding oligotrophic waters (Fig. 6). For Stas. 9 and 11, located at the core of the dome, we found a clear vertical segregation not only between SYN and PRO, but importantly also among specific SYN phylotypes. For instance, Clade II and FLU1A abundances were highest in the surface layer but declined rapidly with depth (Fig. 6). CRD1 and FLU1B were also more abundant in shallow than deeper waters, but they showed a shallow subsurface peak at ~ 20 m depth (Fig. 6). Conversely, Clade XVI increased from near detection limit in the mixed layer to ~ 1000 cells $mL^{-1}$ in a subsurface maxima around ~ 25 m depth (Fig. 6). The abundance of the two main LL adapted PRO clades, FLU2 and FLU3, described a similar vertical pattern with a broad abundance maxima centered at the bottom of the thermocline. This clade-specific distributional pattern leads to a finely structured succession of genetically distinct picocyanobacterial populations that follow the strong physicochemical gradients associated with the dome (Fig. 7). Remarkably, at least three distinguishable SYN populations stacked within the upper 30–40 m of the water column (Fig. 8). FLU1A along with Clade II dominated the thin surface mixed layer typical of the dome. Immediately below, CRD1, accompanied by FLU1B, dominated SYN populations in the upper thermocline. The relative contribution of Clade XVI peaked in the lower thermocline (Fig. 8).

In addition to this vertical partitioning, the distribution of SYN and PRO lineages also differed horizontally across the region, particularly along waters sitting below the mixed layer. For example, Clade XVI and PRO FLU2 populations thrived along the shallow thermocline present in the dome but were virtually absent outside of the dome (Fig. 6), revealing a dramatic shift in community composition below the mixed layer (Fig. 6). Although less marked, differences in the distributions of genetically distinct SYN and PRO populations were also evident in surface waters across the region. For instance, surface concentrations of FLU1A within the dome ($10^5$ cells $mL^{-1}$) were more than two orders of magnitude higher than outside (Fig. 6). In contrast, Clade II abundance increased only moderately toward the dome (Fig. 6). As a result, Clade II clearly dominated surface waters outside the dome (~ 85%), while its relative contribution to SYN assemblage in the center of the dome, although significant (~ 30%), decreased substantially to codominate with FLU1A (Fig. 8). Concentrations of CRD1 and FLU1B were also enhanced by the presence of the dome, particularly at depths just below the thermocline, although the magnitude of this increase was smaller (~ 10-fold) than that observed for FLU1A (Fig. 6).

The different proportions of clone sequences retrieved from surface waters inside and outside of the dome from the FLU1A and FLU1B subclusters (Fig. 4), but especially the distinct qPCR abundance patterns of FLU1A and FLU1B subgroups (Fig. 6), indicate different responses of these closely related subpopulations to the presence of the dome. To explore these relationships, we tracked the abundances of FLU1A and FLU1B in the surface mixed layer along the transect ($n = 13$ Sta.; Fig. 9). Both groups showed increasing concentrations toward the dome, but this trend was more pronounced for FLU1A, which led to a drastic change in the relative proportions of FLU1A and FLU1B in surface waters across the region despite their high genetic similarity inferred from *rpoC1* sequences (Fig. 9).

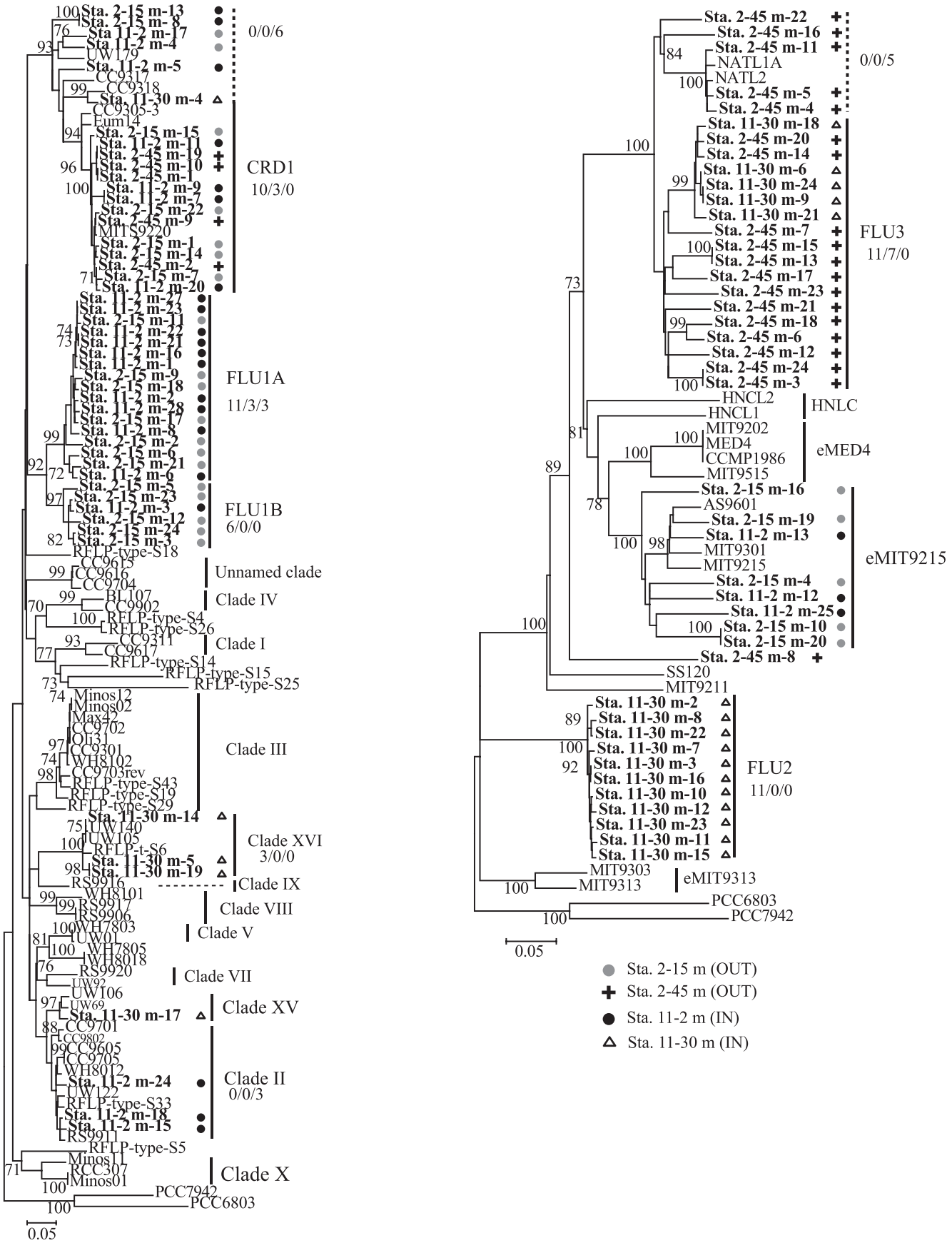
Sta. 2-15 m-13
Sta. 2-15 m- 8
Sta 11-2 m-17
Sta 11-2 m-4
UW179
Sta. 11-2 m-5
CC9317
CC9318
Sta. 11-30 m-4
CC9305-3
Eum14
Sta. 2-15 m-15
Sta. 11-2 m-11
Sta. 2-45 m-19
Sta. 2-45 m-10
Sta. 2-45 m-1
Sta. 11-2 m-9
Sta. 11-2 m-7
Sta. 2-15 m-22
Sta. 2-45 m-9
MITS9220
Sta. 2-15 m-1
Sta. 2-15 m-14
Sta. 2-45 m-2
Sta. 2-15 m-7
Sta. 11-2 m-20
0/0/6
CRD1
10/3/0
Sta. 11-2 m-27
Sta. 11-2 m-23
Sta. 2-15 m-11
Sta. 11-2 m-22
Sta. 11-2 m-21
Sta. 11-2 m-16
Sta. 11-2 m-1
Sta. 2-15 m-9
Sta. 2-15 m-18
Sta. 11-2 m-2
Sta. 11-2 m-28
Sta. 2-15 m-17
Sta. 11-2 m-8
Sta. 2-15 m-2
Sta. 2-15 m-6
Sta. 2-15 m-21
Sta. 11-2 m-6
Sta. 2-15 m-5
Sta. 2-15 m-23
Sta. 11-2 m-3
Sta. 2-15 m-12
Sta. 2-15 m-24
Sta. 2-15 m-3
FLU1A
11/3/3
FLU1B
6/0/0
RFLP-type-S18
CC9615
CC9616
CC9704
BL107
CC9902
RFLP-type-S4
RFLP-type-S26
CC9311
CC9617
RFLP-type-S14
RFLP-type-S15
RFLP-type-S25
Unnamed clade
Clade IV
Clade I
Minos12
Minos02
Max42
CC9702
Oli31
CC9301
WH8102
CC9703rev
RFLP-type-S43
RFLP-type-S19
RFLP-type-S29
Clade III
Sta. 11-30 m-14
UW140
UW105
RFLP-t-S6
Sta. 11-30 m-5
Sta. 11-30 m-19
RS9916
WH8101
RS9917
RS9906
WH7803
UW01
WH7805
WH8018
RS9920
UW92
UW106
UW69
Sta. 11-30 m-17
CC9701
CC9802
CC9605
CC9705
WH8012
Sta. 11-2 m-24
UW122
RFLP-type-S33
Sta. 11-2 m-18
Sta. 11-2 m-15
RS9911
RFLP-type-S5
Minos11
RCC307
Minos01
PCC7942
PCC6803
Clade XVI
3/0/0
Clade IX
Clade VIII
Clade V
Clade VII
Clade XV
Clade II
0/0/3
Clade X
0.05
Sta. 2-45 m-22
Sta. 2-45 m-16
Sta. 2-45 m-11
NATL1A
NATL2
Sta. 2-45 m-5
Sta. 2-45 m-4
0/0/5
Sta. 11-30 m-18
Sta. 2-45 m-20
Sta. 2-45 m-14
Sta. 11-30 m-6
Sta. 11-30 m-24
Sta. 11-30 m-9
Sta. 11-30 m-21
Sta. 2-45 m-7
Sta. 2-45 m-15
Sta. 2-45 m-13
Sta. 2-45 m-17
Sta. 2-45 m-23
Sta. 2-45 m-21
Sta. 2-45 m-18
Sta. 2-45 m-6
Sta. 2-45 m-12
Sta. 2-45 m-24
Sta. 2-45 m-3
FLU3
11/7/0
HNCL2
HNCL1
HNLC
MIT9202
MED4
CCMP1986
MIT9515
eMED4
Sta. 2-15 m-16
AS9601
Sta. 2-15 m-19
Sta. 11-2 m-13
MIT9301
MIT9215
Sta. 2-15 m-4
Sta. 11-2 m-12
Sta. 11-2 m-25
Sta. 2-15 m-10
Sta. 2-15 m-20
eMIT9215
Sta. 2-45 m-8
SS120
MIT9211
Sta. 11-30 m-2
Sta. 11-30 m-8
Sta. 11-30 m-22
Sta. 11-30 m-7
Sta. 11-30 m-3
Sta. 11-30 m-16
Sta. 11-30 m-10
Sta. 11-30 m-12
Sta. 11-30 m-23
Sta. 11-30 m-11
Sta. 11-30 m-15
FLU2
11/0/0
MIT9303
MIT9313
eMIT9313
PCC6803
PCC7942
0.05
Sta. 2-15 m (OUT)
Sta. 2-45 m (OUT)
Sta. 11-2 m (IN)
Sta. 11-30 m (IN)

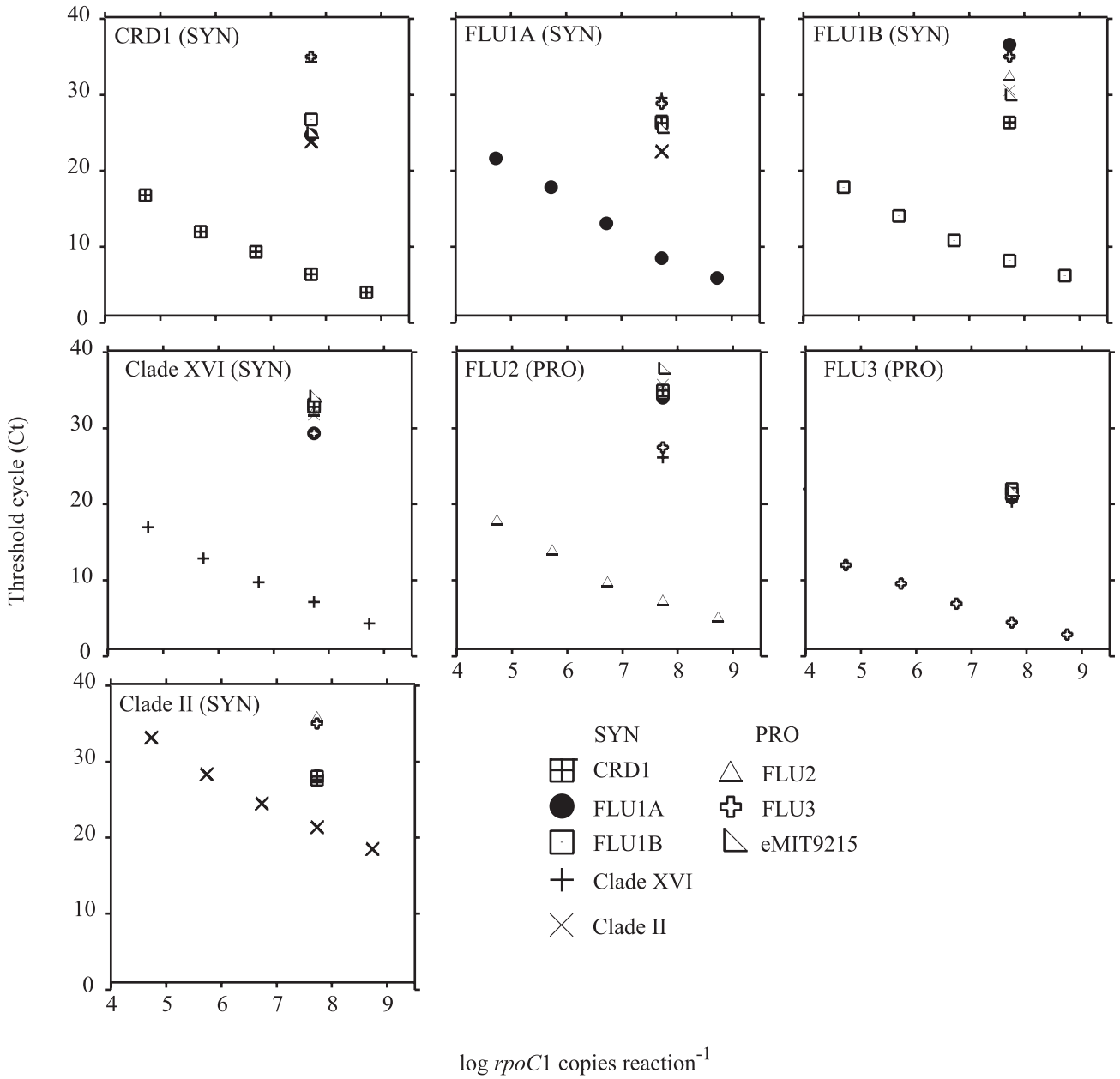


Fig. 5. Cross-reactivity tests performed with target and nontarget plasmid standards for each specific qPCR assay used in this study. Target plasmid standards for each assay are indicated in the upper left corner of each panel.

←

Fig. 4. Maximum likelihood tree of *rpoC1* sequences affiliated to SYN and PRO. The consensus tree was constructed using the TN93 distance model and the 50% majority rule from 1000 bootstrap replicates. Bootstrap values < 70% are not shown. Sequences from environmental libraries collected in this study are in bold and labeled with the station and collection depth followed by a number to designate the environmental clone. Symbols next to these sequences indicate their origin. Both trees were rooted with the PCC7942 and PCC6803 *rpoC1* sequences. Clade and subclade designations are indicated by a solid line. Those targeted by specific qPCR assays in this study are indicated in capital letters, and the numbers shown below refer to the number of sequences with 0/1 to 2/> 2 mismatches with both forward and reverse specific primers designed. Dashed line indicates the fraction of sequences belonging to CRD1 and eNATL2 clades that were not amplified by the corresponding specific primers.

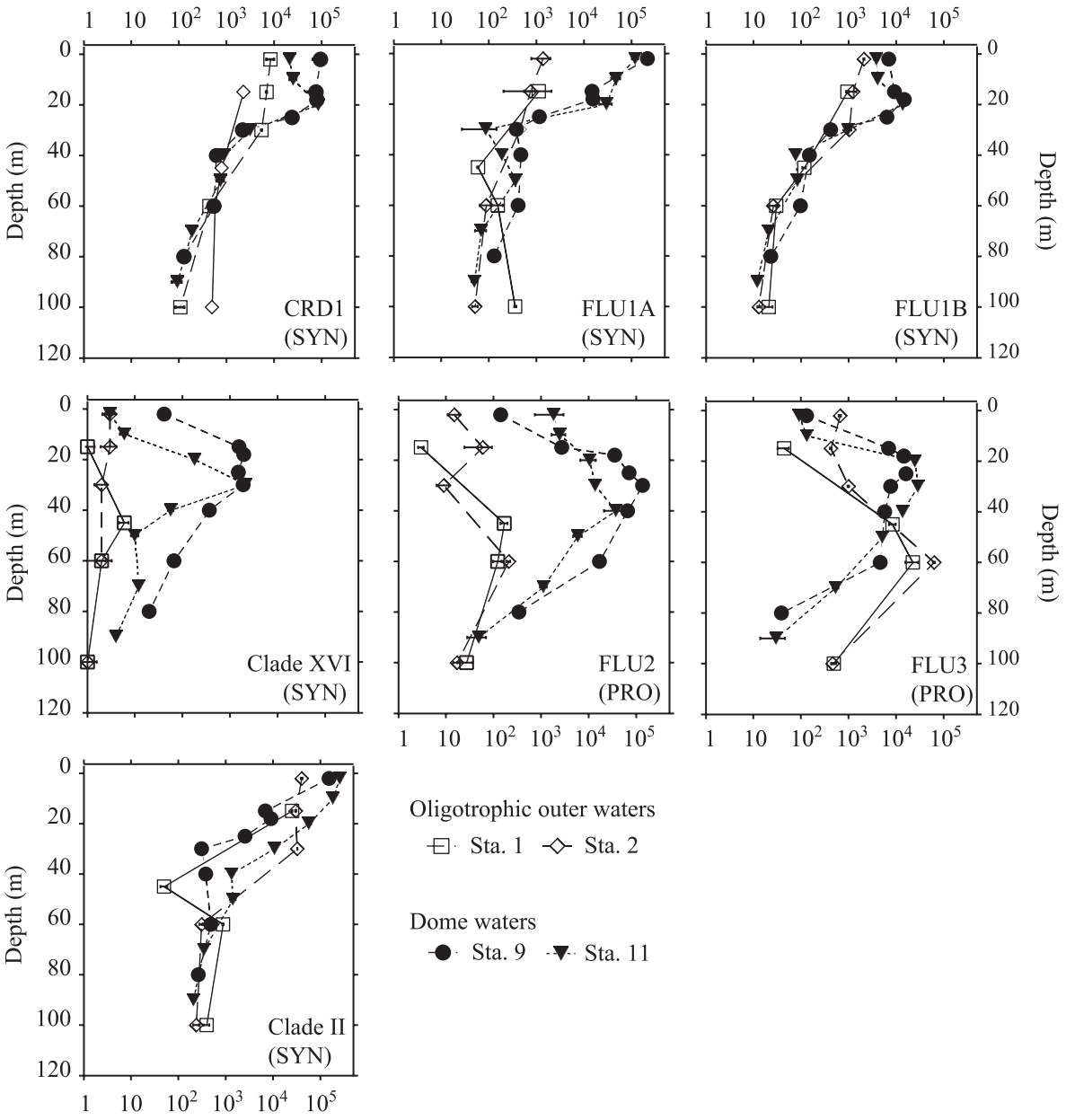


Fig. 6. Vertical abundance distribution of specific SYN and PRO populations across stations within (Stas. 9 and 11) and outside (Stas. 1 and 2) of the dome estimated from specific qPCR assays. Points and error bars represent the means and standard errors of triplicate reactions.

*Environmental factors influencing picocyanobacterial population distributions*—Pairwise correlations between picocyanobacterial subpopulations abundance and environmental variables are shown in Table 2. CRD1, FLU1A, FLU1B, and Clade II were positively correlated with temperature (T), percentage of $I_0$ and oxygen, and inversely correlated with $NO_3^-$ (Table 2), consistent with their higher abundances in shallower waters (Fig. 6). Conversely, Clade XVI, FLU2, and FLU3 were negatively correlated with T and percentage of $I_0$ and positively correlated with $NO_3^-$ and salinity (Table 2), reflecting their deeper distributions (Fig. 6). The abundances of all four SYN genotypes with preference for surface waters (CRD1, FLU1A, FLU1B, and Clade II) were significantly correlated (Table 2). The strength of the relationships was highest between CRD1 and FLU1B (Table 2), which suggested not only the proximity of their ecological niches but also their different environmental preferences relative to Clade II and FLU1A (Fig. 6).

Multidimensional scale ordination of samples based on their specific composition (Fig. 10) is consistent with the fine spatial structure of picocyanobacterial populations revealed by qPCR profiles (Figs. 7, 8) and provides further insights into the physicochemical gradients underlying this spatial complexity. Surface mixed-layer samples were projected in the space characterized by high T and oxygen

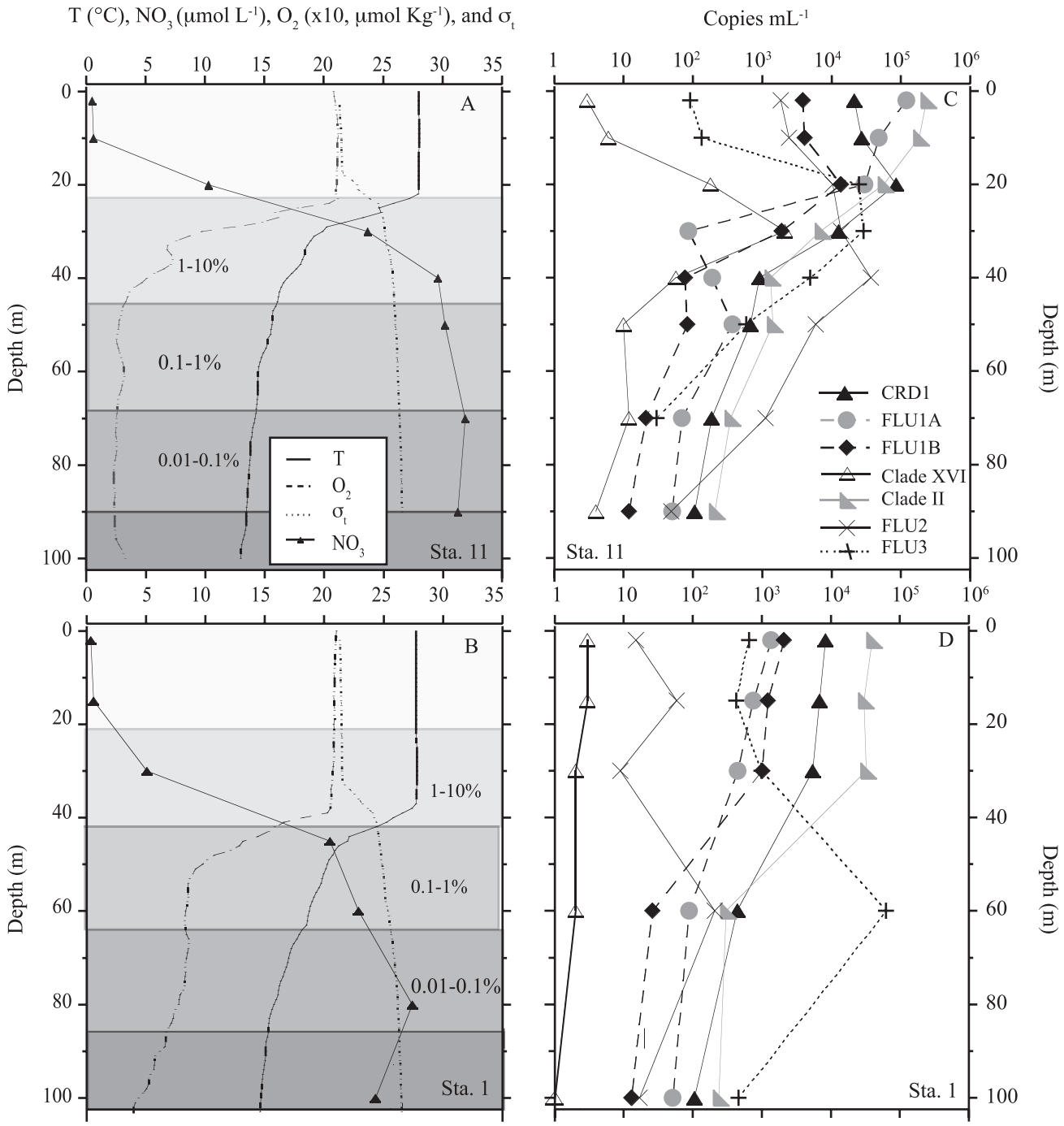


Fig. 7. (A, B) Vertical profiles of temperature (°C), nitrate ($\mu$mol L$^{-1}$), oxygen ($\mu$mol kg$^{-1}$), density ($\sigma_t$), and the percentage of surface irradiance (%$I_0$), (C, D) vertical abundance distribution of specific SYN and PRO populations in Stas. 11 and 1 representative of conditions of the center of the dome and background oligotrophic waters, respectively. (A, B) For the sake of clarity the 0.01–0.1%$I_0$, 0.1–1%$I_0$, and 1–10%$I_0$ photic layers are indicated.

concentrations and further clustered into two separate groups according to their collection within or outside the dome (Fig. 10). The distance to the nitracline ($Z_{nitr}$) seemed the most distinctive environmental property underlying the compositional differences between surface samples (Fig. 8), which otherwise shared similar irradiance, T, and salinity conditions. Samples collected along the upper end of the thermocline within the dome, which aligned with minimum optical depths of the nitracline (high percentage of $I_0 : Z_{nitr}$), shared the distinctive maximum abundance and codominance of CRD1 and FLU1B (Figs. 6, 8). This observation indicates the preference of these groups for intermediate depths, where elevated nutrient-rich waters meet relatively high isolumes (Fig. 7). Finally, samples collected from a deeper portion of the thermocline clustered into two separate groups, one comprising samples from

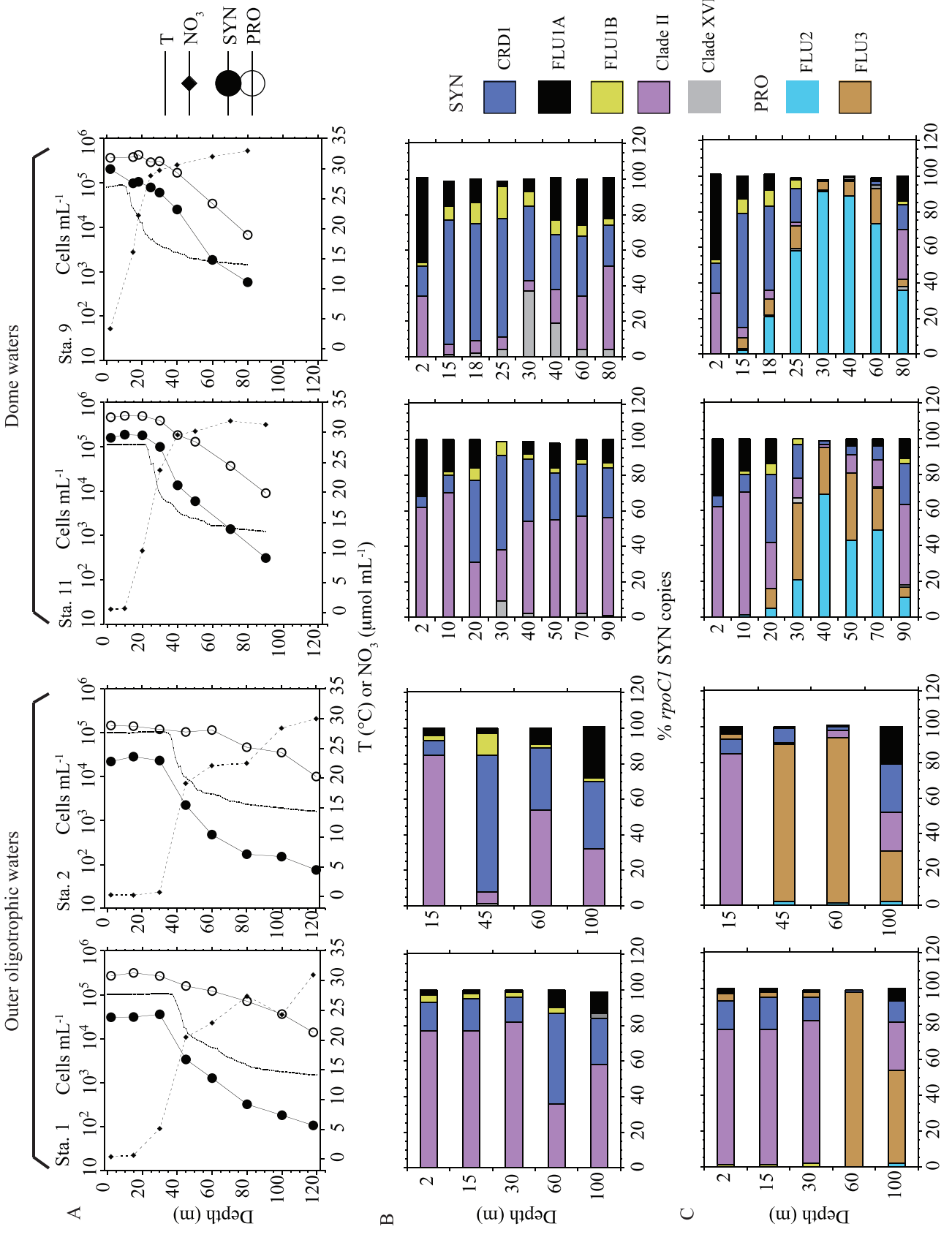


Fig. 8. (A) Vertical profiles of temperature (°C), nitrate ($\mu$mol L$^{-1}$), and SYN and PRO abundances (cells mL$^{-1}$) measured with flow cytometry across stations within (Stas. 9 and 11) and outside the dome (Stas. 1 and 2). Vertical structure of the relative contributions of (B) SYN genotypes to the total SYN assemblage and (C) SYN and PRO specific genotypes to the SYN and PRO picocyanobacterial assemblage. The total SYN *rpoC1* copies and total picocyanobacterial *rpoC1* copies are estimated as the sum of the number of copies for each specific SYN and PRO subpopulations targeted by the specific qPCR assays used in this study.

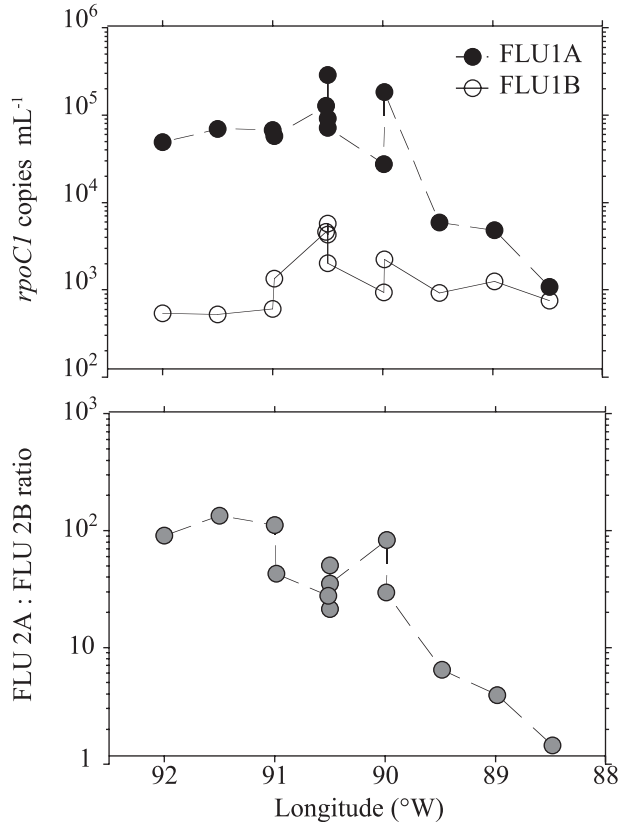


Fig. 9. (A) Abundance of FLU1A and FLU1B (*rpoC1* copies $mL^{-1}$) and (B) the FLU1A : FLU1B abundance ratio in the surface mixed layer along the CRD transect.

low-light low-oxygen waters of the dome, which are clearly dominated by FLU2, and those dominated by FLU3 collected from more oxygenated waters outside the dome (Figs. 8, 10).

## Discussion

*FCM-based picocyanobacterial structure and interannual variability in the CRD*—Abundances of both SYN and PRO, but especially SYN, were markedly enhanced in surface waters in the CRD central upwelling area (Fig. 2). However, although maximum SYN concentrations in our study ($\sim 2 \times 10^5$ cells $mL^{-1}$) were comparable to high values reported in mesotrophic transition zones located off of the Canary upwelling (Partensky et al. 1996; Gutiérrez-Rodríguez et al. 2011) and the Arabian Sea (Campbell et al. 1998; Fuller et al. 2006), they were substantially lower than those reported previously in the CRD ($\sim 10^6$ cells $mL^{-1}$; Li et al. 1983; Saito et al. 2005). This difference is likely due to interannual variability in oceanographic conditions of the CRD, with the most obvious effect being that our study coincided with a mild El Niño event. During our cruise, surface expression of enhanced Chl *a* in the CRD, as visualized in satellite images, was relatively weak compared with high activity years, and sea surface temperature was ~ 1.5°C warmer than reported by Saito et al. (2005). Consistent with PRO preference for warmer and more

Table 2. Spearman correlation between environmental variables, SYN and PRO abundances measured with the flow cytometry, and specific population abundances estimated with qPCR assays. Values shown are the correlation coefficient *p* values between variables. All data used are from Stas. 1, 2, 9, and 11 ($n = 25$). Data were log (x + 1) transformed before analysis. T = temperature, Sal = salinity, $\%I_0$ = percentage of surface irradiance, and $Z_{nitr}$ = nitracline depth.

| | T (°C) | Sal | $\%I_0$ | Oxygen ($\mu$mol $kg^{-1}$) | $NO_3 + NO_2$ ($\mu$mol $L^{-1}$) | $Z_{nitr}$ (m) | Chl *a* ($\mu$g $L^{-1}$) | SYN (cells $mL^{-1}$) | PRO (cells $mL^{-1}$) | CRD1 (copies $mL^{-1}$) | FLU1A (copies $mL^{-1}$) | FLU1B (copies $mL^{-1}$) | Clade II (copies $mL^{-1}$) | Clade XVI (copies $mL^{-1}$) | FLU2 (copies $mL^{-1}$) | FLU3 (copies $mL^{-1}$) |
|---|---|---|---|---|---|---|---|---|---|---|---|---|---|---|---|---|
| T | | <0.0001 | <0.0001 | <0.0001 | <0.0001 | <0.0001 | 0.0122 | 0.0007 | <0.0001 | <0.0001 | 0.0002 | 0.0001 | <0.0001 | 0.4833 | 0.2854 | 0.7589 |
| Sal | −0.87 | | <0.0001 | <0.0001 | <0.0001 | <0.0001 | 0.038 | 0.0015 | 0.0008 | 0.0007 | 0.0021 | 0.0005 | 0.0001 | 0.6672 | 0.1519 | 0.4194 |
| $\%I_0$ | 0.88 | −0.84 | | <0.0001 | <0.0001 | 0.0002 | 0.003 | <0.0001 | <0.0001 | <0.0001 | <0.0001 | <0.0001 | <0.0001 | 0.3435 | 0.7423 | 0.8666 |
| Oxygen | 0.91 | −0.83 | 0.7431 | | <0.0001 | <0.0001 | 0.1198 | 0.0248 | 0.0021 | 0.0048 | 0.0035 | 0.0071 | <0.0001 | 0.0687 | 0.018 | 0.2906 |
| $NO_3 + NO_2$ | −0.94 | 0.86 | −0.80 | −0.97 | | <0.0001 | 0.0806 | 0.0182 | 0.0009 | 0.0014 | 0.0017 | 0.002 | <0.0001 | 0.108 | 0.0309 | 0.4516 |
| $Z_{nitr}$ | 0.84 | −0.81 | 0.68 | 0.85 | −0.87 | | 0.8565 | 0.1865 | 0.0696 | 0.0423 | 0.058 | 0.0405 | 0.0018 | 0.0416 | 0.0054 | 0.0924 |
| Chl *a* | 0.49 | −0.42 | 0.57 | 0.32 | −0.36 | 0.04 | | <0.0001 | <0.0001 | 0.0001 | 0.0013 | 0.0002 | 0.0091 | 0.009 | 0.0075 | 0.0014 |
| SYN fcm | 0.63 | −0.60 | 0.82 | 0.45 | −0.47 | 0.27 | 0.76 | | <0.0001 | <0.0001 | <0.0001 | <0.0001 | <0.0001 | 0.0043 | 0.0268 | 0.4927 |
| PRO fcm | 0.72 | −0.63 | 0.86 | 0.59 | −0.62 | 0.37 | 0.77 | 0.89 | | <0.0001 | <0.0001 | <0.0001 | <0.0001 | 0.034 | 0.1143 | 0.2066 |
| CRD1 | 0.70 | −0.63 | 0.87 | 0.55 | −0.60 | 0.41 | 0.69 | 0.87 | 0.91 | | <0.0001 | <0.0001 | <0.0001 | 0.0143 | 0.1256 | 0.2386 |
| FLU1A | 0.68 | −0.58 | 0.86 | 0.56 | −0.60 | 0.38 | 0.61 | 0.85 | 0.84 | 0.92 | | <0.0001 | <0.0001 | 0.0674 | 0.2479 | 0.858 |
| FLU1B | 0.70 | −0.64 | 0.87 | 0.52 | −0.59 | 0.41 | 0.69 | 0.87 | 0.89 | 0.99 | 0.92 | | <0.0001 | 0.0102 | 0.1285 | 0.2959 |
| Clade II | 0.81 | −0.70 | 0.86 | 0.72 | −0.74 | 0.59 | 0.51 | 0.75 | 0.74 | 0.80 | 0.89 | 0.78 | | 0.8351 | 0.8494 | 0.6822 |
| Clade XVI | −0.15 | 0.09 | 0.20 | −0.37 | 0.33 | −0.41 | 0.51 | 0.55 | 0.43 | 0.48 | 0.37 | 0.50 | 0.04 | | <0.0001 | 0.0182 |
| FLU2 | −0.22 | 0.30 | 0.07 | −0.47 | 0.43 | −0.54 | 0.52 | 0.44 | 0.32 | 0.31 | 0.24 | 0.31 | −0.04 | 0.86 | | 0.0017 |
| FLU3 | −0.06 | 0.17 | −0.04 | −0.22 | 0.16 | −0.34 | 0.60 | 0.14 | 0.26 | 0.24 | 0.04 | 0.22 | −0.09 | 0.47 | 0.59 | |

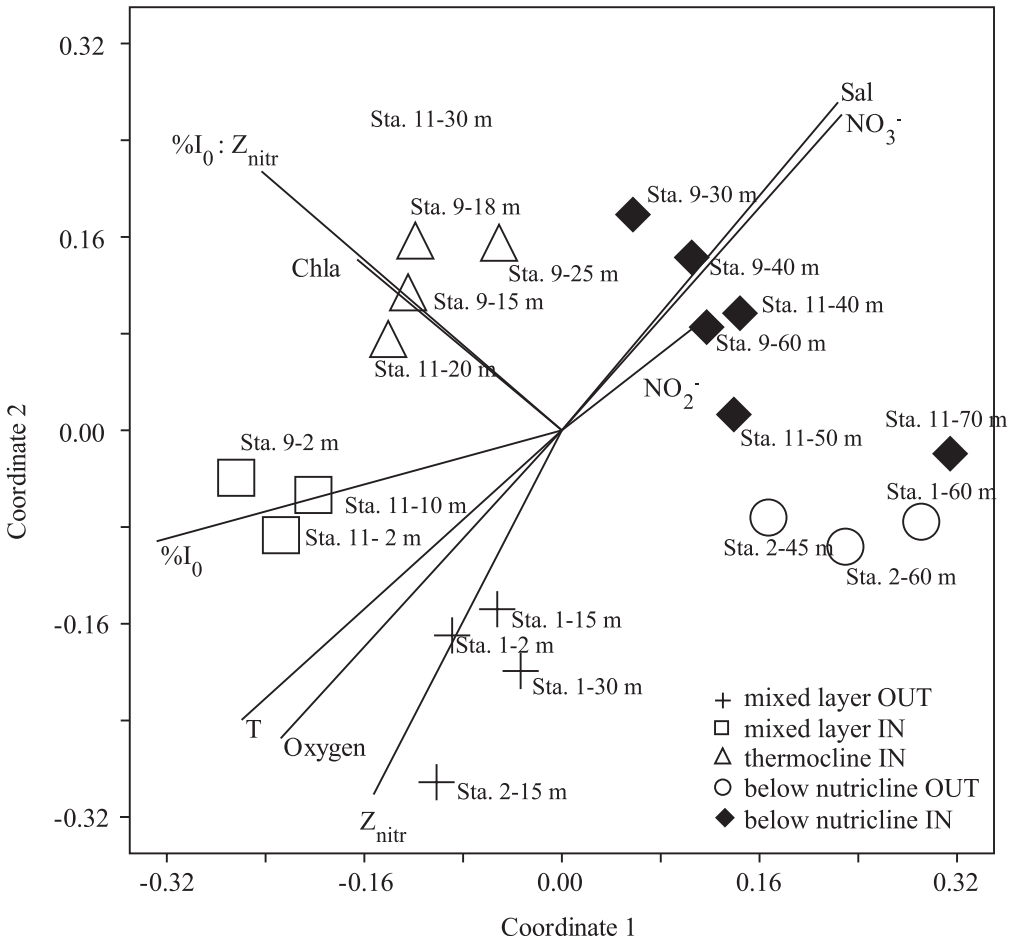


Fig. 10. Nonparametric multidimensional scaling (nMDS) ordination plot of environmental variables and abundances of *rpoC1* subgroups. Samples are labeled based on the station and depths were they were collected. Abbreviations for environmental variables as in Table 2. The length and direction of the vectors projected in the same space represent the strength and sign of the correlation between the environmental variables and the nMDS scores. All data used were log $(x + 1)$ transformed before any analysis.

oligotrophic waters, PRO outnumbered SYN in our study, while Saito et al. (2005) found an order of magnitude more SYN than PRO. In addition to El Niño variability effects (Wang and Fiedler 2006), local atmospheric and oceanic physical processes that drive CRD seasonality (Fiedler 2002) could also have contributed to less than ideal conditions for massive SYN blooms during the time of our study.

A negative relationship between nitracline depth and SYN abundance explains a large fraction of the spatial variability of SYN surface concentrations that we observed in the CRD ($R^2 = 0.64$, $p < 0.01$, $n = 12$ and Fig. 2). More broadly in the Pacific, regions with deep nitraclines, such as the North Pacific subtropical gyre and the western Pacific warm pool, are known to have consistently low SYN abundances (1000–3000 cells $mL^{-1}$; Landry and Kirchman 2002). However, high nitrate concentration in surface waters does not necessarily produce SYN blooms, as is evident by the still modest cell concentrations ($\sim 10^4$ $mL^{-1}$) in iron-limited, high-nitrate waters of the central equatorial Pacific (Landry and Kirchman 2002; Taylor et al. 2011). Nonetheless, it is reasonable to expect years of higher SYN abundance and dominance in the CRD to be associated with a shallower nutricline and increased nutrient delivery. Across onshore–offshore gradients in the California Current Ecosystem (CCE), Collier and Palenik (2003) observed that surface concentrations of SYN reached a maximum at intermediate values of nitracline depth, declining both in absolute abundance and relative to total phytoplankton biomass at upwelling stations closer to the coast. While this suggests that there are limits or nonlinearities in the enhancement effect of nutrient delivery on SYN population response, perhaps due to reduced competitive abilities relative to larger phytoplankton or increased grazing pressure under extreme enrichment, the chemical composition of source waters to the CRD may also be quite different than waters that upwell along the California coast. Owing to the relative paucity of scientific investigations in the CRD, we do not yet know the upper limit to the seasonal bloom in the region or the factors that regulate the response in community composition.

*High clonal diversity in the CRD*—Phylogenetic analysis of clone libraries revealed a remarkably high clonal diversity within the dome, comprising at least four major populations of SYN and three of PRO, and several well-

distinguished subpopulations (Fig. 4). This high diversity suggests that the shoaling of the thermocline not only boosts picocyanobacterial net growth and accumulation, but it also enhances niche diversification, making the CRD a diversity "hot spot" for picocyanobacteria. Using the 16S–23S ribosomal DNA internally transcribed spacer (ITS) as a genetic marker, Saito et al. (2005) reported two major groups, namely, CRD1, closely related to MITS9920, and CRD2 with no cultured representative. Our *rpoC1* clone libraries also revealed two major SYN groups in surface waters of the dome. The close phylogenetic relationship of one group of sequences with MITS9220 and UW179 strongly suggests that it corresponds to CRD1 clade (Fig. 4; Ahlgren and Rocap 2012). Interestingly, CC9305 and other strains recently affiliated to CRD1 (Ahlgren and Rocap 2012) were originally isolated from the California Current using nitrate (Toledo and Palenik 1997), consistent with the presence of closely related phylotypes thriving in the CRD nutrient-rich waters.

Whether FLU1 and CRD2 represent the same SYN group is harder to determine, since they were identified from the analysis of different genes and both groups lack cultured representative isolates to bridge them (Ahlgren and Rocap 2012; Mazard et al. 2012). This being said, it is interesting to note the presence of FLU1 in both mesotrophic and oligotrophic conditions within and outside the dome, respectively (Fig. 4), a pattern consistent with the reported presence of CRD2 in geographically distant sites with contrasting trophic status (Saito et al. 2005; Huang et al. 2011; Ahlgren and Rocap 2012). Analogous trophic flexibility has also been seen for subclades in Clade IV across an onshore–offshore transect in the CCE (Tai et al. 2011). These observations suggest that SYN clades are not always ecologically coherent, but that "subclades" may be the relevant level of phylogenetic discrimination needed (*see* below).

This study reveals a remarkable molecular diversity of picocyanobacterial populations in subsurface waters of the CRD, which harbor a diverse and distinctive assemblage. We found a group of sequences most closely related to UW140 and UW105 strains that define SYN Clade XVI, an observation consistent with the preference for low-light environments suggested for Clade XVI (Ahlgren and Rocap 2006). However, the majority of subsurface sequences from the dome were not closely related to any culture representative or environmental sequence and formed one "novel" picocyanobacterial group, FLU2, which included only sequences retrieved from this environment (Fig. 4). To understand better the specific or general nature of this group, we surveyed publicly available metagenomic datasets in Community Cyberinfrastructure for Advanced Microbial Ecology Research and Analysis (CAMERA) portal (http://camera.calit2.net/index.shtm) using the Basic Local Alignment Search Tool for nucleotide sequences (BLASTn) workflow against "all metagenomic datasets" option. The similarity of FLU2 with the closest 25 hits was significantly lower compared with the similarity values obtained for any other genotype (FLU1, CRD1, Clade II, Clade XVI, FLU3, eMIT9215) subjected to the same analysis ($F_{7,192} = 256.3$, $p < 0.0001$). The distinctive nature of this group is confirmed by this result and by the absence of *rpoC1* sequences affiliated to FLU2 yielded by a local BLASTn performed with the sequences retrieved from the metagenomic datasets survey ($n = 200$) against all environmental and cultured *rpoC1* isolates included in our phylogenetic analysis (Fig. 4). However, the range of natural environmental conditions and ecosystems covered by the currently available metagenomic datasets is still limited, and we cannot, therefore, rule out the presence of the picocyanobacterial diversity represented by FLU2 *rpoC1* groups in other systems not included in metagenomic datasets.

Previous studies have described the presence of a distinctive PRO population in suboxic waters of the lower euphotic zone of the northern Arabian Sea and Pacific waters off Mexico (Johnson et al. 1999; Goericke et al. 2000), at the same depth horizon where eMIT9303 dominates the PRO assemblage in the Arabian Sea (Fuller et al. 2006). Given the close phylogenetic relationship between eMIT9303 and FLU2, the relatively low phylogenetic resolution of the 16S ribosomal DNA molecular marker used by Fuller et al. (2006), and their common preference for low-light suboxic environments, we cannot rule out that FLU2 and eMIT9303 groups represent the same PRO taxa. Furthermore, Lavín et al. (2010) recently reported two low-light, low-oxygen lineages of PRO in the eastern tropical Pacific. Given these observations, we hypothesize that FLU2 in the CRD is closely related to other PRO populations found in the lower euphotic zone of systems with shallow and strong oxygen minimum zones (Goericke et al. 2000; Fuller et al. 2006; Lavín et al. 2010). However, while low-light, low-oxygen populations of PRO described in the Arabian Sea and eastern tropical South Pacific occurred just below the oxycline where oxygen concentrations were $\leq 20$ $\mu$mol $L^{-1}$, FLU2 abundance in the CRD peaked at the bottom of the oxycline at higher oxygen concentration ($\sim 40$ $\mu$mol $L^{-1}$; Fig. 7). Using the specific qPCR assay for the present study, we could not detect FLU2 in deep-chlorophyll samples collected in the same Eastern Pacific region (17°N, 108°W) under similar oceanographic conditions as those surveyed by Goericke et al. (2000). These observations together suggest that despite the general low-light, low-oxygen environmental conditions shared by ecosystems with a strong and shallow oxygen minimum zone (Arabian Sea or Eastern Tropical Pacific), PRO lineages prevailing in the lower euphotic zone are genetically and ecologically distinct despite their phylogenetic proximity.

*Vertical partition of SYN lineages*—A major result of this study is the finely structured vertical partitioning of genetically distinct SYN populations within the Costa Rica Dome (Figs. 7, 8). This is in strong contrast with the generally homogeneous vertical distribution of SYN cell abundance reported elsewhere (Li and Wood 1988; Partensky et al. 1999). Unlike PRO, obvious vertical segregation is generally not observed among SYN lineages, which tend mainly to vary with light and nutrients along horizontal gradients instead (Fuller et al. 2006; Zwirglmaier

et al. 2008; Scanlan et al. 2009). Our results are consistent, however, with a recent report of a subsurface abundance maximum for a SYN genotype in offshore oligotrophic waters of the CCE (Paerl et al. 2011*a*). These results significantly affect current understanding of the factors shaping the structure and function of SYN assemblages in pelagic ecosystems.

Previous studies have described the presence of flow cytometrically different SYN populations below the thermocline across a variety of ecosystems (Olson et al. 1990; Collier and Palenik 2003), but the genetic vs. physiological distinctions of these populations were not resolved. The vertical segregation of SYN genotypes described here was also seen as a succession of SYN populations with different flow-cytometric signatures (high vs. low chlorophyll to PE fluorescence ratios; Fig. 3) at intermediate depths coinciding with the genetically most diverse SYN assemblage. However, the number of molecular populations exceeded those distinguished by flow-cytometric properties. This observation indicates that, despite the consistent pigment variability observed among SYN clones (Wood et al. 1985; Palenik 2001), the large genetic and ecological diversity harbored in natural populations cannot be adequately resolved from optical signatures alone. Overall, our results provide evidence of unprecedented vertical segregation of genetically distinct SYN populations that exhibit a diverse range of optical properties likely relevant to their different ecological niches.

The fine vertical structure of picocyanobacterial populations in the central CRD (Figs. 7, 8) aligns with distinct euphotic zone habitats formed by isotherm compression and sharp physicochemical gradients (Fig. 7). Inside and outside of the dome, the nitracline and oxycline are located in very different ranges of optical depths (Fig. 7). Based on the magnitude of this difference and the importance of light-nutrient interactions suggested by nMDS analysis (Fig. 10), one can envision the key role that bringing such physicochemical gradients into significantly higher irradiance fields could have on structuring photosynthetic communities. In addition to greater availability of oxidized nitrogen forms, potentially used by both SYN and PRO populations (Casey et al. 2007; Martiny et al. 2009*a*,*b*), the shallow nitracline is likely associated with enhanced supply of micronutrients to the euphotic zone. Previous studies have noted that trace-metal chemistry likely plays a key role in determining SYN abundances (Saito et al. 2005; Rivers et al. 2009) as well as eukaryotic phytoplankton dynamics in the CRD (Franck et al. 2003). For instance, Saito et al. (2005) reported that net growth rate of total SYN increase in response to Co and Co + Fe addition, while SYN fluorescence per cell responded to Fe and Co + Fe additions. During our cruise, SYN abundances paralleled variations in total Fe and Fe(II) concentrations measured across the region (J. Moffett pers. comm.). More recently, Rivers et al. (2009) explored the Fe stress status of bulk SYN in the CRD using a novel immunofluorescence bioassay. The authors observed that the degree of Fe limitation exhibited by SYN was finely structured along the Fe vertical gradient measured within the euphotic zone, in a similar fashion to the vertical partitioning of genetically distinct populations that we observed in this study. In fact, this genetic diversity confounds the interpretation of the SYN Fe limitation variability observed by Rivers et al. (2009), since it could reflect physiological and/or taxonomic changes. Little is known about the clade-specific response of SYN to different trace-metal availability, although several lines of evidence suggest distinct metal-related ecophysiology among strains (Palenik et al. 2006; Barnett et al. 2012).

*Horizontal variability of picocyanobacterial populations across the CRD*—Although less marked, our study also revealed different horizontal distribution patterns for genetically distinct subpopulations of SYN and PRO across small scales (Fig. 6) that lead to significantly different picocyanobacterial assemblages *in* and *out* of the dome (Fig. 8). The overall high concentration of Clade II across the CRD (Fig. 6) is in good agreement with its reported presence in warm subtropical and tropical waters (Ferris and Palenik 1998; Zwirglmaier et al. 2008). However, the only previous SYN diversity survey available for the CRD did not find Clade II clones in surface waters ($\sim$ 8 m; Saito et al. 2005). This discrepancy can be explained by the stacked vertical structure of SYN populations unveiled here, which shows a sharp decrease in the abundance and relative contribution of Clade II accompanied by an increase in CRD1 below the shallow thermocline of the dome (Figs. 7, 8). Similarly, the contradictory picture arising when comparing the dominance of Clade II that we observed in surface waters of the dome (2 m) with the dominance of CRD1 clones reported by Saito et al. (2005) in surface waters (8 m) can be reconciled based on the vertical partitioning of SYN populations described here.

The current study reveals a complex horizontal distribution pattern for Clade II. On one hand, the surface concentration of this group increased toward mesotrophic waters of the dome (Fig. 6), in good agreement with its reported capacity to thrive under nutrient-rich upwelling conditions (Fuller et al. 2006; Zwirglmaier et al. 2008). On the other hand, this increase in absolute abundance is paralleled by a decreasing relative contribution to total SYN (Fig. 8). This pattern derives mainly from the response of FLU1A and to a minor extent CRD1, which are strongly favored by the ecological conditions associated with the upwelling waters, whereas Clade II seems less responsive to the presence of the dome (Fig. 6). One could argue that the high concentrations of Clade II across contrasting regions *in* and *out* of the dome could reflect changes in Clade XV concentrations overlooked by Clade II specific qPCR assay. However, the fact that all clones obtained from the library built with the qPCR product of Clade II specific assays were indeed affiliated to Clade II argues against this methodological explanation for the high concentrations of Clade II across contrasting trophic conditions in the CRD region and highlights again the ecological flexibility that can be found at clade-level taxonomic resolution.

*Taxonomic resolution and ecological significance of SYN subpopulations*—The huge genetic diversity comprised

by SYN is thought to foster its ubiquitous distribution and ability to thrive across contrasting environmental conditions (Scanlan et al. 2009). The different distributional patterns of SYN populations across environmental gradients of the CRD (Figs. 7, 8) are consistent with this idea and provide further evidence of the ecophysiological diversity encompassed by distinct genotypes. The use of high-resolution molecular markers often reveals the presence of numerous subpopulations within SYN and PRO major clades (Martiny et al. 2009*b*; Huang et al. 2011; Mazard et al. 2012). Whether this microdiversity represents coexisting ecologically differentiated genomes, however, remains an open question (Acinas et al. 2004). Recent studies of the role of horizontal gene transfer in *Synechococcus* clade diversity suggest that this microdiversity has ecological relevance (Stuart et al. 2013).

The spatial partitioning of picocyanobacterial clades across contrasting oceanographic conditions (Fuller et al. 2006; Paerl et al. 2011*a*; Ahlgren and Rocap 2012) and the general consistency of the basin-scale distributions of SYN clades (Zwirglmaier et al. 2007, 2008) may link genetic and ecological diversity at this level of taxonomic resolution. However, following the same rationale, the marked differences between the FLU1A and FLU1B dynamics across the CRD (Fig. 9) would argue against the ecological homogeneity of at least some SYN clades. Along these lines, a recent sampling of a coastal–to–open-ocean transect across the California Current has shown distinct distributional patterns for closely related SYN subclades (Tai et al. 2011). Moreover, the reported presence of SYN clades such as CRD2 and Clade II in ecosystems with different physicochemical parameters further suggests that subclades within these clades might be important to their success.

Martiny et al. (2009*b*) observed that the significance of specific environmental variables on PRO diversity depended on the taxonomic resolution they used to compartmentalize this diversity. For instance, light and nutrients were the most determinant factors when broader genetic resolution was investigated, while dispersal time arose as the relevant factor for finer taxonomic resolution (Martiny et al. 2009*b*). Phylogenetic analysis of the FLU3 group, most closely related to the low-light–adapted eNATL2 (Fig. 4), provides further opportunity to consider the ecological significance of within-clade microdiversity. Because of its ability to thrive in high surface waters, eNATL2 is thought to be an "intermediate" clade (Coleman and Chisholm 2007; Zinser et al. 2007; Partensky and Garczarek 2010). Consistent with this ability, FLU3 reached similar maximum concentrations at different optical depths *in* ($\sim$ 10%$I_0$) and *out* of the dome ($\sim$ 0.1%$I_0$; Fig. 7). Interestingly, FLU3 comprised two subgroups with different proportions of sequences retrieved from waters in and outside the dome (Fig. 4). These observations lead us to wonder whether the intermediate nature of eNATL2 reflects the physiological flexibility of a genetically homogeneous group (Coleman and Chisholm 2007) or the presence of genetically distinct subpopulations with different ecophysiological properties (Martiny et al. 2009*b*).

With qPCR, our study has revealed consistent differences in spatial distributions of closely related SYN subpopulations vertically and horizontally (Figs. 6–9). Given the seasonal nature of the CRD, these spatial segregations may result from dynamic responses of subpopulations already present in background oligotrophic waters prior to the development of the dome, as opposed to populations transported to the dome region by offshore transport of coastal blooms. Our results, as well as others (Martiny et al. 2009*b*; Tai et al. 2011; Ahlgren and Rocap 2012), illustrate the ecological diversity hidden within clades and, therefore, highlight the importance of defining the appropriate level of taxonomic resolution for addressing fundamental questions about the distribution, function, and evolution of SYN and PRO populations.

In addition to environmental forcing, biotic interactions such as viral infection (Mühling et al. 2005) and protistan grazing (Apple et al. 2011) can greatly influence diversity and dynamics of picocyanobacterial populations. Given the strong viral and grazing mortality pressure exerted upon picocyanobacterial populations (Baudoux et al. 2008), specific differences affecting the outcome of these processes are likely to affect the dynamics and succession of natural populations as much as the more frequently invoked bottom-up forces. There is therefore an urgent need to measure process rates at appropriate taxonomic resolution if we aim to understand fully the mechanisms driving picocyanobacterial diversity in the field.

*Acknowledgments*

We thank the captain, crew, and restechs of the R/V *Melville*. We are grateful to all of our colleagues in the Flux and Zinc Experiments (FLUZiE) Program, particularly Rhona Stuart, Michael Stukel, Steven Baines, Moira Décima, Tak Kataoka, C. J. Bradley, Ally Pasulka, Andrew Taylor, and Dan Wick, for their help at sea and in the lab. We thank Ralf Goericke for sharing samples collected in Pacific waters off Mexico for picocyanobacterial population analysis, as well as Chris L. Dupont and Douglas B. Rusch for providing the *Prochlorococcus marinus* HNLC1-2 *rpoC1* nucleotide sequence. We thank Ryan Paerl and two anonymous reviewers for insightful comments and suggestions. This work was supported by National Science Foundation (NSF) grants OCE-0826626 (MRL) and MCB0744334 (BP), and by a Ramon Areces Foundation fellowship to AGR.

## References

Acinas, S. G., V. Klepac-Ceraj, D. E. Hunt, C. Pharino, I. Ceraj, D. L. Distel, and M. F. Polz. 2004. Fine-scale phylogenetic architecture of a complex bacterial community. Nature **430:** 551–554, doi:10.1038/nature02649

Ahlgren, N. A., and G. Rocap. 2006. Culture isolation and culture-independent clone libraries reveal new marine *Synechococcus* ecotypes with distinctive light and N physiologies. Appl. Environ. Microbiol. **72:** 7193–7204, doi:10.1128/AEM.00358-06

———, and ———. 2012. Diversity and distribution of marine *Synechococcus*: Multiple gene phylogenies for consensus classification and development of qPCR assays for sensitive measurement of clades in the ocean. Front. Microbiol **3:** 1–24, doi:10.3389/fmicb.2012.00213

Apple, J. K., S. L. Strom, B. Palenik, and B. Brahamsha. 2011. Variability in protist grazing and growth on different marine *Synechococcus* isolates. Appl. Environ. Microbiol. **77:** 3074–3084, doi:10.1128/AEM.02241-10

Barnett, J. P., A. Millard, A. Z. Ksibe, D. J. Scanlan, R. Schmid, and C. A. Blindauer. 2012. Mining genomes of marine cyanobacteria for elements of zinc homeostasis. Front. Microbiol **3:** 1–21, doi:10.3389/fmicb.2012.00142

Baudoux, A. C., M. J. W. Veldhuis, A. A. M. Noordeloos, G. Van Noort, and C. P. D. Brussaard. 2008. Estimates of virus- vs. grazing induced mortality of picophytoplankton in the North Sea during summer. Aquat. Microb. Ecol **52:** 69–82, doi:10.3354/ame01207

Campbell, L., M. R. Landry, J. Constantinou, H. A. Nolla, S. L. Brown, H. Liu, and D. A. Caron. 1998. Response of microbial community structure to environmental forcing in the Arabian Sea. Deep-Sea Res. II **45:** 2301–2325, doi:10.1016/S0967-0645(98)00072-1

Casey, J. R., M. W. Lomas, J. Mandecki, and D. E. Walker. 2007. *Prochlorococcus* contributes to new production in the Sargasso Sea deep chlorophyll maximum. Geophys. Res. Lett. **34:** 1–5.

Coleman, M. L., and S. W. Chisholm. 2007. Code and context: *Prochlorococcus* as a model for cross-scale biology. Trends Microbiol. **15:** 398–407, doi:10.1016/j.tim.2007.07.001

Collier, J. L., and B. Palenik. 2003. Phycoerythrin-containing picoplankton in the Southern California Bight. Deep-Sea Res. II **50:** 2405–2422, doi:10.1016/S0967-0645(03)00127-9

Doolittle, D. F., W. K. W. Li, and A. M. Wood. 2008. Wintertime abundance of picoplankton in the Atlantic sector of the Southern Ocean. Nova Hedwigia **133:** 147–160.

Edgar, R. C. 2004. MUSCLE: Multiple sequence alignment with high accuracy and high throughput. Nucleic Acids Res. **32:** 1792–1797, doi:10.1093/nar/gkh340

Ferris, M. J., and B. Palenik. 1998. Niche adaptation in ocean cyanobacteria. Nature **396:** 226–228, doi:10.1038/24297

Fiedler, P. C. 2002. The annual cycle and biological effects of the Costa Rica Dome. Deep-Sea Res. I **49:** 321–338.

———, and L. D. Talley. 2006. Hydrography of the eastern tropical Pacific: A review. Prog. Oceanogr. **69:** 143–180, doi:10.1016/j.pocean.2006.03.008

Franck, V., K. Bruland, D. Hutchins, and M. Brzezinski. 2003. Iron and zinc effects on silicic acid and nitrate uptake kinetics in three high-nutrient, low-chlorophyll (HNLC) regions. Mar. Ecol. Prog. Ser. **252:** 15–33, doi:10.3354/meps252015

Fuller, N. J., D. Marie, D. Vaulot, A. F. Post, and D. J. Scanlan. 2003. Clade-specific 16S ribosomal DNA oligonucleotides reveal the predominance of a single marine *Synechococcus* clade throughout a stratified water column in the Red Sea. Appl. Environ. Microbiol. **69:** 2430–2443, doi:10.1128/AEM.69.5.2430-2443.2003

———, G. A. Tarran, M. Yallop, K. M. Orcutt, and D. J. Scanlan. 2006. Molecular analysis of picocyanobacterial community structure along an Arabian Sea transect reveals distinct spatial separation of lineages. Limnol. Oceanogr. **51:** 2515–2526, doi:10.4319/lo.2006.51.6.2515

Goericke, R., R. J. Olson, and A. Shalapyonok. 2000. A novel niche for *Prochlorococcus* sp. in low-light suboxic environments in the Arabian Sea and the Eastern Tropical North Pacific. Deep-Sea Res. I **47:** 1183–1205, doi:10.1016/S0967-0637(99)00108-9

Gutiérrez-Rodríguez, A., M. Latasa, S. Agustí, and C. M. Duarte. 2011. Distribution and contribution of major phytoplankton groups to carbon cycling across contrasting conditions of the subtropical northeast Atlantic Ocean. Deep-Sea Res. I **58:** 1115–1129, doi:10.1016/j.dsr.2011.08.003

Hammer, Ø., D. A. T. Harper, and P. D. Ryan. 2001. PAST: Paleontological statistics software Package for education and data analysis. Palaeontologia Electronica **4:** 1–9 [accessed 29 January 2014]. Available from http://palaeo-electronica.org/2001_1/past/issue1_01.htm

Hou, Y., H. Zhang, L. Miranda, and S. Lin. 2010. Serious overestimation in quantitative PCR by circular (supercoiled) plasmid standard: Microalgal pcna as the model gene. PLoS One **5:** e9545, doi:10.1371/journal.pone.0009545

Huang, S., S. W. Wilhelm, H. R. Harvey, K. Taylor, N. Jiao, and F. Chen. 2011. Novel lineages of *Prochlorococcus* and *Synechococcus* in the global oceans. ISME J. **6:** 285–297, doi:10.1038/ismej.2011.106

Jardillier, L., M. V. Zubkov, J. Pearman, and D. J. Scanlan. 2010. Significant $CO_2$ fixation by small prymnesiophytes in the subtropical and tropical northeast Atlantic Ocean. ISME J. **4:** 1180–1192, doi:10.1038/ismej.2010.36

Johnson, Z., and others. 1999. Energetic and growth kinetics of a deep *Prochlorococcus* population in the Arabian Sea. Deep-Sea Res. II **46:** 1719–1743, doi:10.1016/S0967-0645(99)00041-7

Landry, M. R., and D. L. Kirchman. 2002. Microbial community structure and variability in the tropical Pacific. Deep-Sea Res. II **49:** 2669–2694, doi:10.1016/S0967-0645(02)00053-X

———, M. D. Ohman, R. Goericke, M. R. Stukel, and K. Tsyrklevich. 2009. Lagrangian studies of phytoplankton growth and grazing relationships in a coastal upwelling ecosystem off Southern California. Prog. Oceanogr. **83:** 208–216, doi:10.1016/j.pocean.2009.07.026

Lavín, P., B. González, J. F. Santibáñez, D. J. Scanlan, and O. Ulloa. 2010. Novel lineages of *Prochlorococcus* thrive within the oxygen minimum zone of the eastern tropical South Pacific. Environ. Microbiol. Rep. **2:** 728–738, doi:10.1111/j.1758-2229.2010.00167

Li, W. K. W. 1994. Primary production of prochlorophytes, cyanobacteria, and eucaryotic ultraphytoplankton: Measurements from flow cytometric sorting. Limnol. Oceanogr. **39:** 169–175, doi:10.4319/lo.1994.39.1.0169

———, D. V. S. Rao, W. G. Harrison, J. C. Smith, J. J. Cullen, B. Irwin, and T. Platt. 1983. Autotrophic picoplankton in the tropical ocean. Science **219:** 292–295, doi:10.1126/science.219.4582.292

———, and A. M. Wood. 1988. Vertical distribution of North Atlantic ultraphytoplankton: Analysis by flow cytometry and epifluorescence microscopy. Deep-Sea Res. **35:** 1615–1638, doi:10.1016/0198-0149(88)90106-9

Martiny, A. C., S. Kathuria, and P. M. Berube. 2009*a*. Widespread metabolic potential for nitrite and nitrate assimilation among *Prochlorococcus* ecotypes. Proc. Natl. Acad. Sci. USA **106:** 10787–10792, doi:10.1073/pnas.0902532106

———, A. P. K. Tai, D. Veneziano, F. Primeau, and S. W. Chisholm. 2009*b*. Taxonomic resolution, ecotypes and the biogeography of *Prochlorococcus*. Environ. Microbiol. **11:** 823–832, doi:10.1111/j.1462-2920.2008.01803

Mazard, S., M. Ostrowski, F. Partensky, and D. J. Scanlan. 2012. Multi-locus sequence analysis, taxonomic resolution and biogeography of marine *Synechococcus*. Environ. Microbiol. **14:** 372–386, doi:10.1111/j.1462-2920.2011.02514

Moore, L. R., and S. W. Chisholm. 1999. Photophysiology of the marine cyanobacterium *Prochlorococcus*: Ecotypic differences among cultured isolates. Limnol. Oceanogr. **44:** 628–638, doi:10.4319/lo.1999.44.3.0628

Mühling, M., and others. 2005. Genetic diversity of marine *Synechococcus* and co-occurring cyanophage communities: Evidence for viral control of phytoplankton. Environ. Microbiol. **7:** 499–508, doi:10.1111/j.1462-2920.2005.00713

———, and ———. 2006. High resolution genetic diversity studies of marine *Synechococcus* isolates using *rpoC1*-based restriction fragment length polymorphism. 2006. Aquat. Microb. Ecol. **45:** 263–275, doi:10.3354/ame045263

Olson, R. J., S. W. Chisholm, E. R. Zettler, and E. V. Armbrust. 1990. Pigments, size, and distribution of *Synechococcus* in the North Atlantic and Pacific Oceans. Limnol. Oceanogr. **35:** 45–58, doi:10.4319/lo.1990.35.1.0045

Paerl, R. W., K. S. Johnson, R. M. Welsh, A. Z. Worden, F. P. Chavez, and J. P. Zehr. 2011*a*. Differential distributions of *Synechococcus* subgroups across the California Current System. Front. Microbiol. **2:** 1–22, doi:10.3389/fmicb.2011.00059

———, K. A. Turk, R. A. Beinart, F. P. Chavez, and J. P. Zehr. 2011*b*. Seasonal change in the abundance of *Synechococcus* and multiple distinct phylotypes in Monterey Bay determined by rbcL and narB quantitative PCR. Environ. Microbiol. **14:** 580–593, doi:10.1111/j.1462-2920.2011.02594

Palenik, B. 1994. Cyanobacterial community structure as seen from RNA polymerase gene sequence analysis. Appl. Environ. Microbiol. **60:** 3212–3219.

———. 2001. Chromatic adaptation in marine *Synechococcus* strains. Appl. Environ. Microbiol. **67:** 991–994, doi:10.1128/AEM.67.2.991

———, and others. 2006. Genome sequence of *Synechococcus* CC9311: Insights into adaptation to a coastal environment. Proc. Natl. Acad. Sci. USA **103:** 13555–13559, doi:10.1073/pnas.0602963103

Partensky, F., J. Blanchot, F. Lantoine, J. Neveux, and D. Marie. 1996. Vertical structure of picophytoplankton at different trophic sites of the tropical northeastern Atlantic Ocean. Deep-Sea Res. I **43:** 1191–1213, doi:10.1016/0967-0637(96)00056-8

———, ———, and D. Vaulot. 1999. Differential distribution and ecology of *Prochlorococcus* and *Synechococcus* in oceanic waters, p. 457–475. *In* L. C. and A. Larkum [eds.], Marine cyanobacteria. Musee Oceanographique.

———, and L. Garczarek. 2010. *Prochlorococcus*: Advantages and limits of minimalism. Ann. Rev. Mar. Sci. **2:** 305–331, doi:10.1146/annurev-marine-120308-081034

Post, A. F., S. Penno, K. Zandbank, A. S. Paytan, M. Huse, and D. M. Welch. 2011. Long term seasonal dynamics of *Synechococcus* population structure in the Gulf of Aqaba, northern Red Sea. Front. Microbiol. **2:** 1–12, doi:10.3389/fmicb.2011.00131

Rivers, A. R., R. W. Jakuba, and E. A. Webb. 2009. Iron stress genes in marine *Synechococcus* and the development of a flow cytometric iron stress assay. Environ. Microbiol. **11:** 382–396, doi:10.1111/j.1462-2920.2008.01778

Rocap, G., D. L. Distel, J. B. Waterbury, and S. W. Chisholm. 2002. Resolution of *Prochlorococcus* and *Synechococcus* ecotypes by using 16S-23S ribosomal DNA internal transcribed spacer sequences. Appl. Environ. Microbiol. **68:** 1180–1191, doi:10.1128/AEM.68.3.1180

———, and others. 2003. Genome divergence in two *Prochlorococcus* ecotypes reflects oceanic niche differentiation. Nature **424:** 1042–1047, doi:10.1038/nature01947

Saito, M. A., G. Rocap, and J. W. Moffett. 2005. Production of cobalt binding ligands in a *Synechococcus* feature at the Costa Rica upwelling dome. Limnol. Oceanogr. **50:** 279–290, doi:10.4319/lo.2005.50.1.0279

Scanlan, D. J., and N. J. West. 2002. Molecular ecology of the marine cyanobacterial genera *Prochlorococcus* and *Synechococcus*. FEMS Microbiol. Rev. **40:** 1–12, doi:10.1111/j.1574-6941.2002.tb00930.x

———, and others. 2009. Ecological genomics of marine picocyanobacteria. Microbiol. Mol. Biol. Rev. **73:** 249–299, doi:10.1128/MMBR.00035-08

Schlitzer, R. 2006. Ocean Data View [accessed 29 January 2014]. Available from http://odv.awi.de.

Selph, K. E., and others. 2011. Spatially-resolved taxon-specific phytoplankton production and grazing dynamics in relation to iron distributions in the Equatorial Pacific between 110 and 140°W. Deep-Sea Res. II **58:** 358–377, doi:10.1016/j.dsr2.2010.08.014

Stuart, R. K., B. Brahamsha, K. Busby, and B. Palenik. 2013. Genomic islands in a coastal marine *Synechococcus* strain confer enhanced tolerance to copper and oxidative stress. ISME J. **7:** 1139–1149, doi:10.1038/ismej.2012.175

Tai, V., R. Burton, and B. Palenik. 2011. Temporal and spatial distributions of marine *Synechococcus* in the Southern California Bight assessed by hybridization to bead-arrays. Mar. Ecol. Prog. Ser. **426:** 133–147, doi:10.3354/meps09030

———, and B. Palenik. 2009. Temporal variation of *Synechococcus* clades at a coastal Pacific Ocean monitoring site. ISME J. **3:** 903–915, doi:10.1038/ismej.2009.35

Tamura, K., and M. Nei. 1993. Estimation of the number of nucleotide substitutions in the control region of mitochondrial DNA in humans and chimpanzees. Mol. Biol. Evol. **10:** 512–526.

———, D. Peterson, N. Peterson, G. Stecher, M. Nei, and S. Kumar. 2011. MEGA5: Molecular evolutionary genetics analysis using maximum likelihood, evolutionary distance, and maximum parsimony methods. Mol. Biol. **28:** 1530–1534, doi:10.1093/molbev/msr121

Taylor, A. G., M. R. Landry, K. E. Selph, and E.-J. Yang. 2011. Biomass, size structure and depth distributions of the microbial community in the eastern equatorial Pacific. Deep-Sea Res. II **58:** 342–357, doi:10.1016/j.dsr2.2010.08.017

Toledo, G., and B. Palenik. 1997. *Synechococcus* diversity in the California current as seen by RNA polymerase (*rpoC1*) gene sequences of isolated strains. Appl. Environ. Microbiol. **63:** 4298–4303.

Wang, C., and P. C. Fiedler. 2006. ENSO variability and the eastern tropical Pacific: A review. Prog. Oceanogr. **69:** 239–266, doi:10.1016/j.pocean.2006.03.004

Waterbury, J. B., S. W. Watson, R. R. L. Guillard, and L. E. Brand. 1979. Widespread occurrence of a unicellular, marine, planktonic cyanobacterium. Nature **277:** 293–294, doi:10.1038/277293a0

Wood, A. M., P. K. Horan, K. Muirhead, D. A. Phinney, C. M. Yentsch, and J. B. Waterbury. 1985. Discrimination between types of pigments in marine *Synechococcus* spp. by scanning spectroscopy, epifluorescence microscopy, and flow cytometry. Limnol. Oceanogr. **30:** 1303–1315, doi:10.4319/lo.1985.30.6.1303

Wyrtki, K. 1964. Upwelling in the Costa Rica Dome. Fish. Bull. **63:** 355–372.

Zinser, E. R., Z. I. Johnson, A. Coe, D. Veneziano, and S. W. Chisholm. 2007. Influence of light and temperature on *Prochlorococcus* ecotype distributions in the Atlantic Ocean. Limnol. Oceanogr. **52:** 2205–2220, doi:10.4319/lo.2007.52.5.2205

Zwirglmaier, K., J. L. Heywood, K. Chamberlain, E. M. S. Woodward, M. V. Zubkov, and D. J. Scanlan. 2007. Basin-scale distribution patterns of picocyanobacterial lineages in the Atlantic Ocean. Environ. Microbiol. **9:** 1278–1290, doi:10.1111/j.1462-2920.2007.01246.x

———, and others. 2008. Global phylogeography of marine *Synechococcus* and *Prochlorococcus* reveals a distinct partitioning of lineages among oceanic biomes. Environ. Microbiol. **10:** 147–161, doi:10.1111/j.1462-2920.2007.01440

*Associate editor: Wade H. Jeffrey*

*Received: 29 May 2013*
*Accepted: 04 December 2013*
*Amended: 07 January 2014*